THE JOURNAL OF BIOLOGICAL CHEMISTRY VOL. 283, NO. 27, pp. 19095–19111, July 4, 2008

Cellular Functions of Human RPA1

*MULTIPLE ROLES OF DOMAINS IN REPLICATION, REPAIR, AND CHECKPOINTS**

Received for publication, February 1, 2008, and in revised form, May 5, 2008 Published, JBC Papers in Press, May 9, 2008, DOI 10.1074/jbc.M800881200

Stuart J. Haring, Aaron C. Mason, Sara K. Binz[1], and Marc S. Wold[2]

From the Department of Biochemistry, Carver College of Medicine, University of Iowa, Iowa City, Iowa 52242

In eukaryotes, the single strand DNA (ssDNA)-binding protein, replication protein A (RPA), is essential for DNA replication, repair, and recombination. RPA is composed of the following three subunits: RPA1, RPA2, and RPA3. The RPA1 subunit contains four structurally related domains and is responsible for high affinity ssDNA binding. This study uses a depletion/replacement strategy in human cells to reveal the contributions of each domain to RPA cellular functions. Mutations that substantially decrease ssDNA binding activity do not necessarily disrupt cellular RPA function. Conversely, mutations that only slightly affect ssDNA binding can dramatically affect cellular function. The N terminus of RPA1 is not necessary for DNA replication in the cell; however, this region is important for the cellular response to DNA damage. Highly conserved aromatic residues in the high affinity ssDNA-binding domains are essential for DNA repair and cell cycle progression. Our findings suggest that as long as a threshold of RPA-ssDNA binding activity is met, DNA replication can occur and that an RPA activity separate from ssDNA binding is essential for function in DNA repair.

Cell survival and proliferation depend on the efficient maintenance of genetic information. Human cells must accurately replicate billions of base pairs of DNA and identify and repair a wide variety of DNA lesions. One of the proteins required for the maintenance of genomic integrity is replication protein A (RPA).[3] RPA is a heterotrimeric single strand DNA (ssDNA)-binding protein, composed of 70-, 32-, and 14-kDa subunits, commonly referred to as RPA1, RPA2, and RPA3, respectively (1–3). Homologs of the three RPA subunits have been found in all eukaryotes examined (1, 4). The major biochemical activity of RPA is ssDNA binding; RPA can bind ssDNA with subnanomolar affinity (5). The ability of RPA to bind ssDNA is not sequence-specific; however, RPA has a higher affinity for pyrimidine-rich and telomeric ssDNA (6–8).

Replication protein A was originally isolated as a factor essential for *in vitro* DNA replication of simian virus 40 (SV40) (9–11), and it has since been shown to be essential for a number of other DNA metabolic processes, including chromosomal DNA replication, repair, and recombination (1–3). RPA also has a role in maintenance of telomeres (7, 12) and in regulation of the cell cycle (13, 14). The common feature of all of these processes is that each has ssDNA intermediates that must be recognized and processed appropriately. RPA interacts with ssDNA in the cell and with a number of proteins involved in these processes (3, 15).

Each of the RPA subunits has at least one domain containing an oligonucleotide/oligosaccharide-binding (OB) fold. This fold is found in many ssDNA- and sugar-binding proteins (16). The OB-folds in RPA are commonly referred to as DNA-binding domains (DBDs). RPA1 contains four OB-folds, and RPA2 and RPA3 have one OB-fold each. Although each OB-fold is structurally similar, the majority of the ssDNA binding occurs through two OB-folds (DBD-A and DBD-B) centrally located in RPA1, referred to as the ssDNA-binding core (17, 18). The ssDNA-binding core is both necessary and sufficient for high affinity DNA binding (17–19). In addition to the ssDNA-binding core, RPA1 contains an OB-fold at each terminus. The N terminus of RPA1, containing DBD-F, has been implicated in DNA repair, recombination, and cell cycle regulation in yeast (13, 20, 21). This may be due to the large number of known protein interactions with RPA through the N-terminal region of RPA1 (2, 22). The C terminus of RPA1, containing DBD-C, interacts with DNA, is required for complex formation, and has been implicated in recognition of DNA damage (23, 24). RPA2 contains an OB-fold (DBD-D) that can be cross-linked to DNA at the primer-template junction (25) and is involved in heterotrimeric complex formation (23). RPA3 is composed exclusively of an OB-fold (DBD-E) that interacts with DBD-C of RPA1 and DBD-D of RPA2 to form a heterotrimeric complex (26, 27).

Deletion analysis of RPA in *Saccharomyces cerevisiae* has revealed the regions of Rfa1, Rfa2, and Rfa3 (RPA1, RPA2, and RPA3, respectively, in yeast) essential for viability. In yeast, the OB-folds of each subunit comprise the minimal essential regions for each protein (28). Additionally, screens for mutations of *RFA1* and *RFA2* with various sensitivities (*e.g.* MMS, UV, Ts) have been performed, and one mutation that has been of particular interest is the *rfa1-t11* mutation (20). This mutation is located in the N-terminal region (DBD-F) of Rfa1. *rfa1-t11* mutants display the ability to replicate DNA and divide;

* This work was supported, in whole or in part, by National Institutes of Health Grant GM44721 (to M. S. W.). This work was also supported by American Heart Association Postdoctoral Fellowship 0525735Z (to S. J. H.). The costs of publication of this article were defrayed in part by the payment of page charges. This article must therefore be hereby marked "*advertisement*" in accordance with 18 U.S.C. Section 1734 solely to indicate this fact.

[1] Present address: Dept. of Biochemistry and Molecular Biophysics, Washington University, St. Louis, MO 63110.

[2] To whom correspondence should be addressed: University of Iowa, Carver College of Medicine, Dept. of Biochemistry, 3107 MERF, Iowa City, IA 52242. Tel.: 319-335-6784; Fax: 319-384-4770; E-mail: marc-wold@uiowa.edu.

[3] The abbreviations used are: RPA, replication protein A; RNAi, RNA interference; ssDNA, single strand DNA; DBD, DNA-binding domain; CPT, camptothecin; ETP, etoposide; DMEM, Dulbecco's modified Eagle's medium; siRNA, short interfering RNA; BCS, bovine calf serum; WT, wild type; GFP, green fluorescent protein; PBS, phosphate-buffered saline; DAPI, 4′,6-diamidino-2-phenylindole; UTR, untranslated region; TBS, Tris-buffered saline; ATM, ataxia telangiectasia mutated.

however, they also display moderate to severe phenotypes in response to cellular stresses (20, 29–39).

Depletion of RPA1 in human cells has been shown to lead to a number of phenotypes. First, it appears that depletion of RPA1 has no discernible effect on RPA2 protein levels in the cell (14, 40). Cells lacking RPA1 have been reported to have slower S phase progression followed by an arrest in G_2/M, and RPA1 knockdown also leads to formation of γ-H2AX foci (14). The G_2/M arrest observed is ATM-dependent, as it is alleviated by depletion of ATM (14). It has also been demonstrated that RPA1 depletion leads to phosphorylation of Chk2 (in addition to ATM) and activation of p21 expression (40). The phosphorylation of Chk2 is alleviated by ATM depletion or by caffeine treatment (40). This is not surprising as Chk2 is a downstream target of ATM (41). In addition to ATM activation, RPA1 is necessary for association of the Rad9-Rad1-Hus1 (9-1-1) complex with damaged DNA (42).

All of the above phenotypes are caused by the lack of the entire RPA1 protein; however, it is not clear what regions of RPA1 are important for RPA function in the human cell and what features of RPA1 contribute to the observed phenotypes. To identify this, one must examine mutant forms of the protein within the cell. In this study, we utilized a knockdown and replacement strategy to identify domain contributions and to correlate biochemical properties of RPA1 with effects on cellular function. We examined mutations in the core ssDNA-binding region and in domains that do not contribute substantially to ssDNA binding to understand what contribution each domain makes to RPA function. The results confirm that depletion of RPA1 does not affect RPA2 or RPA3 levels in the cell. Furthermore, loss of RPA1 can result in G_2/M arrest but also causes a severe S phase defect. Mutants in the core ssDNA-binding region have the most substantial effects on cellular function; however, these effects are not strictly correlated with ssDNA binding affinity. In fact, a mutation that reduces ssDNA binding by two orders of magnitude does not appear to affect RPA1 function. Conversely, mutations in highly conserved aromatic residues in the ssDNA-binding core reduce ssDNA binding by less than an order of magnitude, yet lead to checkpoint activation and cell cycle arrest. A form of RPA that has the C-terminal domain of RPA1 (DBD-C) deleted is unable to support DNA replication. However, deletion of the N-terminal region of RPA1 (DBD-F) reveals that this region is not essential for DNA replication and that its only function may be in response to cellular stress.

EXPERIMENTAL PROCEDURES

RNAi Knockdown of Endogenous RPA1—To knock down endogenous RPA1, a short interfering RNA (siRNA) was synthesized (Dharmacon) to target the 3′-untranslated region (UTR) of RPA1. The target sequence of the RPA1 siRNA was 5′-GGAAUUAUGUCGUAAGUCA-3′. HeLa cells grown in DMEM supplemented with 10% bovine calf serum (BCS) were seeded at 2×10^5 cells per well in 6-well tissue culture plates. After 16–24 h of growth at 37 °C with 5% CO_2, cells were transfected with 200 pmol of RPA1 siRNA using 5 μl of Lipofectamine 2000 (Invitrogen) per well. After 16–24 h of growth following siRNA transfection, the media were removed, and 2 ml of DMEM, 10% BCS was added to each well.

Examination of RNAi Knockdown by Immunoblot Analysis—At various times following RNAi knockdown, the media from each well were removed, and the remaining attached cells were trypsinized. The trypsinized cells were pelleted at $1.25 \times g$ for 5 min at room temperature. The cells were washed once with phosphate-buffered saline (PBS; 137 mM NaCl, 2.7 mM KCl, 4.3 mM $Na_2HPO_4 \cdot 7H_2O$, 1.4 mM KH_2PO_4), and Abraham's lysis buffer (50 mM HEPES·NaOH (pH 7.5), 1% Triton X-100, 150 mM NaCl, 30 mM sodium pyrophosphate, 1 mM EDTA, 10 mM sodium fluoride, 1 mM sodium vanadate, 10 μg/ml pepstatin A, 0.04 μg/ml microcystin, 5 μg/ml aprotinin, 10 μg/ml leupeptin, 2 mM PMSF) was added to lyse the cells. The samples were stored at −80 °C. Samples were thawed and sonicated four times for 2.5 s at setting 4 with 5 s between each sonication using a Sonic Dismembrator 550 (Fisher). The protein in the cell lysate was quantitated using the DC assay (Bio-Rad), and 80 μg of total protein was loaded onto an 8–14% gradient SDS-polyacrylamide gel and run at 35 watts for 1.25 h. The gel was transferred to Trans-Blot transfer medium (pure nitrocellulose; Bio-Rad) at 0.1 mA for 16–20 h. The membrane was blocked with 10% nonfat dry milk, 1× TBS, 0.1% Tween 20 for 30–60 min. The blocking solution was removed, and primary antibody in 1× TBS, 0.1% Tween 20 was added to the membrane and incubated at room temperature for 2 h overnight. Primary antibodies used were 2H10 (mouse monoclonal anti-RPA1:70c (43)), 71-9A (mouse monoclonal antibody anti-RPA2:71 (44)), and N2.2 (rabbit polyclonal antibody) at 1:7,500, 1:15,000, and 1:500, respectively. The membrane was then washed three times with 1× TBS, 0.1% Tween 20. The secondary antibody goat anti-mouse IgG horseradish peroxidase (Sigma) or goat anti-rabbit IgG horseradish peroxidase (Sigma) was diluted 1:20,000 in 1× TBS, 0.1% Tween 20, added to the membrane, and incubated for 1–2 h at room temperature. The membrane was washed four times with 1× TBS, 0.1% Tween 20. SuperSignal West Pico chemiluminescent substrate (Pierce) was used to detect horseradish peroxidase.

Construction of Epitope-tagged RPA Expression Plasmids—To allow for detection of exogenous RPA, GFP-tagged versions of RPA1, RPA2, and RPA3 were generated. The plasmids pEGFP-hsRPA70, pEGFP-hsRPA32, and pEGFP-hsRPA14 were generated by PCR amplification of the RPA1, RPA2, and RPA3 coding regions from p11d-tRPA (45). Primers used were as follows: O-522 (5′-CCCGCGGTACCTCACATCAATGCACTTCTC-CTGATG-3′) and O-519 (5′-GACTCAGATCTGGTGGAG-GCATGGTCGGCCAGCTG-3′) to amplify RPA1; O-578 (5′-CAGATCTCGAGGTGGAGGCATGTGGAACAGTGG-ATTCGAAAG-3′) and O-575 (5′-CCCGCGGTACCTTATT-CTGCATCTGTGGATTTAAAATGG-3′) to amplify RPA2; and O-583 (5′-GCGGCAGATCTGGTGGAGGCATGGTGG-ACATGATGGACTTGCCC-3′) and O-584 (5′-CCCGCGGT-ACCTCAATCATGTTGCACAATCCC-3′) to amplify RPA3. The RPA1 and RPA3 coding region containing fragments were cloned into the BglII-KpnI sites of pEGFP-C1 (Clontech). The RPA2 coding region containing fragment was cloned into the XhoI-KpnI sites of pEGFP-C1. All constructs were confirmed by DNA sequencing.

To generate mutant RPA expression constructs, p11d-tRPA·70(R234A/E277A) (17), which directs the expression of all three subunits of RPA, was used as a template for *in vitro* site-directed mutagenesis using the QuikChange multisite-directed mutagenesis kit (Stratagene). The primer used to generate p11d-tRPA·70(R234A/K263A/E277A) (RPA1-TM) mutations was O-429 (5′-CTTGTTAGCAATCGCCAGGGTCCCTTTCGCCAAATA-3′). Primers O-429 and O-441 (5′-CCCTTCCCCGGCGGAGTTGCT-3′) were used to generate p11d-tRPA·70(R216A/R234A/K263A/E277A) (RPA1-QM). The primers O-429, O-441, and O-425 (5′-TTGCTTCCCTTCGCCGGCGGAGTTGCTCGCGGTCGCGATCTGACTTTGT-3′) were used to generate p11d-tRPA·70(R210A/W212A/R216A/R234A/K263A/E277A) (RPA1-CM). To generate the RPA1-t11 mutation, the QuikChange XL site-directed mutagenesis kit (Stratagene) was used with primers O-502 (5′-ACTCATGAGCAGTCGGAATTCCGGCGGACTATTCCC-3′) and O-503 (5′-GGGAATAGTCCGCCGGAATTCCGACTGCTCATGAGT-3′) and p11d-tRPA (45) as the DNA template. All mutations were confirmed by DNA sequencing.

GFP-tagged RPA1-DM (K263A and E277A), RPA1-TM (R234A, K263A, and E277A), RPA1-QM (R216A, R234A, K263A, and E277A), RPA1-CM (R210A, W212A, R216A, R234A, K263A, and E277A), and RPA1-aroA (F238A and F269A) and mutant constructs were generated by cloning the PstI-XhoI fragments encompassing these mutations from the appropriate bacterial RPA expression vectors into pEGFP-hsRPA70. GFP-RPA1-aroB (W361A and F386A) was generated similarly to pEGFP-RPA70, except P11d-tRPA70 (W361A and F386A) was used as the template. To generate the GFP-RPA1-ΔFL (deletion of first 168 amino acids), the appropriate region was PCR-amplified from p11d-tRPA·70ΔN168 (46) with primers O-640 (5′-GCGGCAGATCTGGTGGAGGCATGGCAGGTCCCAGCCTGTCACAC-3′) and O-522, and this fragment was cloned into BglII-KpnI of pEGFP-C1. The GFP-tagged RPA1-t11 (R41E and Y42F) mutant was generated using the QuikChange XL site-directed mutagenesis kit (Stratagene) with primers O-502 (5′-ACTCATGAGCAGTCGGAATTCCGGCGGACTATTCCC-3′) and O-503 (5′-GGGAATAGTCCGCCGGAATTCCGACTGCTCATGAGT-3′) and pEGFP-hsRPA70 as a DNA template. pEGFP-hsRPA70 was also mutagenized with primers O-505 (5′-CTAAAGAGCGGCGGCCGCGGAGGGAGTAAC-3′) and O-546 (5′-GTTACTCCCTCCGCGGCCGCCGCTCTTTAG-3′) to generate a unique NotI site between DBD-B and DBD-C (pEGFP-hsRPA70-N). Primers O-766 (5′-GGCCGTGGAGGGAGTAACACCAACTGATAGTAAGAATTCGGTAC-3′) and O-767 (5′-CGAATTCTTACTATCAGTTGGTGTTACTCCCTCCAC-3′) were then annealed, and this linker was cloned into the NotI-KpnI sites of pEGFP-hsRPA70-N to generate pEGFP-hsRPA70-ΔC. All mutations were confirmed by DNA sequencing.

Expression and Purification of RPA and ssDNA Binding Analysis—Purification of RPA and mutant forms of RPA were performed as described in Henricksen *et al.* (45) and Binz *et al.* (47).

To determine ssDNA-binding constants for mutant and wild-type (WT) forms of RPA, an oligonucleotide (dT_{30}) was labeled with [γ-^{32}P]ATP by T4 polynucleotide kinase (New England Biolabs). The labeled DNA was separated from free ATP with a P-30 Micro Bio-Spin Tris chromatography column (Bio-Rad). Each ssDNA-binding reaction contained 1× FBB (30 mM HEPES (pH 7.8), 100 mM NaCl, 5 mM $MgCl_2$, 0.5% inositol, 1 mM dithiothreitol), 2 fmol of ssDNA, bovine serum albumin (50 μg/μl), and the indicated amount of mutant or WT RPA (0–3000 fmol). Wild-type RPA was added to a reaction mixture containing 0.2 fmol of radiolabeled ssDNA. The binding reaction was incubated for 20 min at 25 °C. The reactions were then brought to a final concentration of 4% glycerol and 0.01% bromphenol blue and separated on a 1% agarose gel in 0.1% TAE buffer. The gels were then dried onto DE81 paper, and radioactive bands were visualized by autoradiography and quantitated using the Packard Instant Imager. The binding isotherms, used to calculate binding constants, were generated by plotting the fraction of free ssDNA *versus* RPA concentration in each reaction. The intrinsic binding constants were calculated by nonlinear least squares fitting of the data to the Langmuir binding equation using Kaleidagraph (Synergy Software) as described previously (48).

Expression of Exogenous RPA Mutant Constructs in Cells—RNAi was performed as described to knock down endogenous RPA1. At 24 h post-transfection of siRNA, cells were transfected with 250 ng of GFP-RPA1 (WT or mutant) plasmid using 5 μl of Lipofectamine 2000 (Invitrogen) per well. At 48 h post-transfection of siRNA (24 h post-transfection of exogenous RPA1 plasmid), the media were removed, and 2 ml DMEM, 10% BCS was added to each well.

Localization of RPA after CPT or ETP Treatment by Immunofluorescence Microscopy—HeLa cells grown in DMEM, 10% BCS were seeded at 2–4 × 10^5 cells per well on coverslips in 6-well tissue culture plates. RNAi and transfection of plasmid were performed as described to knock down endogenous RPA1 and express exogenous RPA1. At 92 h post-transfection of siRNA, CPT was added to each well to a final concentration of 2 μM, or ETP was added to a final concentration of 20 μM. The cells were incubated at 37 °C, 5% CO_2 for 4 h. The coverslips were washed with cold CSK (10 mM HEPES (pH 7.4), 300 mM sucrose, 100 mM NaCl, 3 mM $MgCl_2$·$6H_2O$) twice and then treated with CSK, 0.5% Triton X-100 (with 1 mM PMSF, 1 mM sodium vanadate, 1 μg/ml aprotinin) for 5 min. Coverslips were then fixed with 4% formaldehyde. After 20 min, the coverslips were washed one time with PBS, treated with 0.5% NP40 in PBS for 5 minutes, and washed three times with PBS. To detect endogenous RPA1, the coverslips were incubated in Blocking solution (2% BSA, 1% normal goat serum, PBS) for 30 min. Primary antibody (2H10) diluted 1:500 in Blocking solution was added to each well containing a coverslip, and the coverslips were incubated for 2–4 h. The coverslips were then washed with PBS three times. Secondary antibody (goat anti-mouse IgG fluorescein isothiocyanate) was diluted 1:800 in Blocking solution and added to the coverslips for 1 h in the dark. The coverslips were incubated in DNA staining solution (1 μg/ml 4′,6-diamidino-2-phenylindole (DAPI), PBS), washed, and mounted to slides. For detection of exogenous GFP-tagged RPA1, the primary and secondary antibody steps were omitted.

Cells were examined using a Leica immunofluorescence microscope. Images of nuclei were collected using SPOT software (Diagnostic Instruments, Inc.) and Photoshop (Adobe) was used to pseudo-color the images.

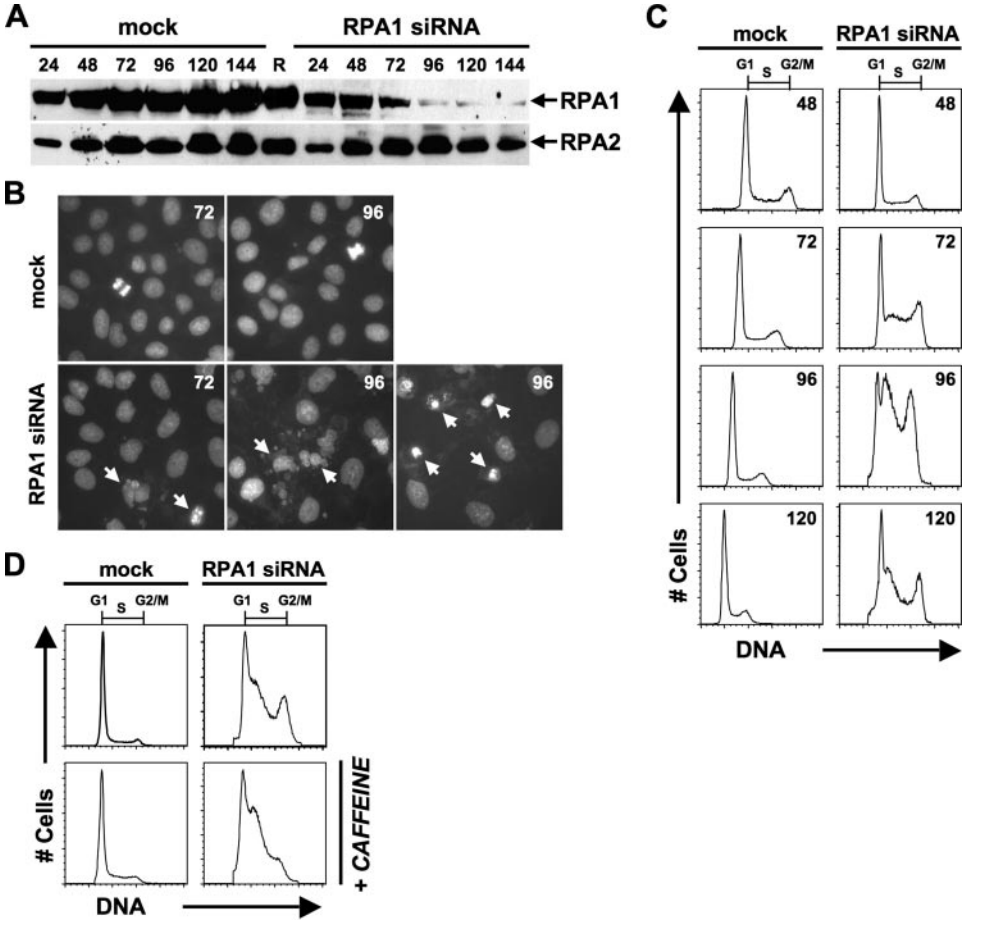

FIGURE 1. **Knockdown of RPA1 in HeLa cells.** *A,* Western blot showing time course of RPA1 siRNA knockdown and mock depletion and effects on the RPA2 subunit. Number of hours post-transfection of siRNA are denoted *above* each lane. The *lane labeled R* (RPA) is 100 ng of purified recombinant human RPA. The blot was first probed with 2H10 to detect RPA1 and then stripped and reprobed with 71-9A to detect RPA2. *B,* microscopic examination of RPA1-depleted cells. Cells were DAPI-stained at 72 and 96 h (designated *72* or *96* in *upper right corner* of each panel) post-transfection of RPA1 siRNA or after mock transfection. *Upper panels* are mock-transfected cells showing intact nuclei and some mitotic nuclei. *Lower panels* are RPA1-depleted. *Arrows* designate fragmented, aberrant, and micronuclei formation. *C,* cell cycle analysis of RPA1 siRNA knockdown. Cells were analyzed by flow cytometry. DNA content was plotted as number of cells (*y* axis labeled *# Cells*) *versus* red (FL2-A) fluorescence (*x* axis labeled *DNA*). Cells with unreplicated DNA content are labeled as G_1 phase, cells with replicated DNA content are labeled G_2/M phase, cells with intermediate DNA content are labeled S phase. The number of hours post-transfection of siRNA is designated in the *upper right corner* of each histogram. Mock- and RPA1 siRNA-transfected samples are designated *above* the histograms. *D,* cell cycle analysis of cells treated with caffeine. At 72 h after mock transfection or post-transfection of RPA1 siRNA, 3 mM caffeine was added, and cells were incubated for 24 h. At 96 h, cells were collected and analyzed as in *C*.

Induction of DNA Damage and G_2/M Arrest in Cells for Flow Cytometric Analysis using CPT or ETP—RNAi and transfection of plasmid DNA were performed as described to knock down endogenous RPA1 and express exogenous RPA1. To examine establishment/maintenance of the G_2/M checkpoint, CPT was added to the cells to a final concentration of 0.1 μM, or ETP was added to a final concentration of 4 μM, at 48 h post-transfection of siRNA. The cells were incubated at 37 °C, 5% CO_2 for 48 h. At 96 h post-transfection of siRNA, the cells were collected for flow cytometric analysis. To examine if mutants have a phenotype at lower levels of CPT or ETP, cells were treated with 0.01 μM CPT or 0.4 μM ETP (10-fold lower concentrations) at 48 h post-transfection of siRNA and incubated at 37 °C/5% CO_2 for an additional 48 h.

Cell Cycle and γ-H2AX Analysis by Flow Cytometry—RNAi and transfection of plasmid DNA were performed as described to knock down endogenous RPA1 and express exogenous RPA1. At various times following RNAi knockdown cells were collected. The collected cells were washed once with PBS and fixed and permeabilized 1 h to overnight in 70% methanol. The fixed cells were pelleted at 1.25 × *g* for 5 min, and 1 ml of PBS was added to each tube. The cells were incubated at room temperature for 1–2 h. The rehydrated cells were pelleted at 1.25 × *g* for 5 min, and 150 μl of RNase A solution (1 mg/ml RNase, PBS) was added to each tube, and the cells were incubated at 4 °C for 1–2 h. Finally, 150 μl of propidium iodide solution (0.1 mg/ml propidium iodide, PBS) was added to each tube. Cells were examined within 1–3 days on a FACSCalibur (BD Biosciences) using FlowJo software (TreeStar). Quantitation of the cell cycle was performed using the Cell Cycle analysis tool in FlowJo.

To detect differences in γ-H2AX staining in cells containing different forms of RPA1, cells were transfected and fixed in methanol as described above. The cells were then rehydrated in PBS, washed, and resuspended in Blocking solution for 30 min. Primary antibody (rabbit anti-γ-H2AX; Calbiochem) was diluted 1:800 in Blocking solution and added to the cells and incubated for 2–4 h. The cells were then washed with PBS two times. Secondary antibody (goat anti-rabbit IgG-APC) was diluted 1:20 in Blocking solution and added to the cells for 1 h in the dark. The cells were washed twice with PBS and examined by flow cytometry.

RESULTS

RNAi Knockdown of RPA1 in Human Cells Leads to a Replication Defect—To characterize the effects of RPA1 depletion in human cells, RNAi was utilized to target RPA1 mRNA for degradation. Examination of RPA1 knockdown by RNAi reveals that RPA1 is a stable protein, as depletion of RPA1 protein levels was not detected until 72 h ($t = 72$) after transfection with RPA1 siRNA (Fig. 1*A*). Maximal knockdown of RPA1 protein occurs at 96 h ($t = 96$) post-transfection (Fig. 1*A*). Similar to other studies of RPA1 knockdown (14, 40), there is no effect on RPA2 protein levels (Figs. 1*A* and 2*D*). Microscopic examination of cells at 72 h post-transfection of RPA1 siRNA reveals some nuclear fragmentation observed as micronuclei forma-

TABLE 1
Cell cycle analysis of RPA1 knockdown and complementation by RPA1 mutant constructs using the Watson pragmatic model

siRNA	Exogenous RPA mutant	Mutation(s)	% of cells in G_1 phase	% of cells in S phase	% of cells in G_2/M phase
None	None		63 ± 4	27 ± 4	10 ± 3
RPA1	None		18 ± 7	66 ± 6	15 ± 3
RPA1	WT		61 ± 4	29 ± 2	8 ± 1
RPA1	RPA1-DM	K263A E277A	56 ± 9	32 ± 4	9 ± 3
RPA1	RPA1-TM	R234A K263A E277A	49 ± 3	36 ± 1	12 ± 3
RPA1	RPA1-QM	R216A R234A K263A E277A	46 ± 9	38 ± 6	14 ± 0
RPA1	RPA1-CM	R210A W212A R216A R234A K263A E277A	16 ± 6	75 ± 3	6 ± 2
RPA1	RPA1-aroA	F238A F269A	40 ± 8	35 ± 5	22 ± 1
RPA1	RPA1-aroB	W361A F386A	19 ± 5	47 ± 11	32 ± 8
RPA1	RPA1-t11	R41E Y42F	63 ± 5	25 ± 2	9 ± 2
RPA1	RPA1-ΔFL	Δ1–168	58 ± 12	29 ± 4	9 ± 4
RPA1	RPA1-ΔC	Δ442–616	13 ± 10	65 ± 2	15 ± 2

tion (Fig. 1*B*). At 96 h post-transfection of RPA1 siRNA, even more nuclear fragmentation is observed, and fewer cells remain adherent (Fig. 1*B*).

One obvious prediction is that depletion of RPA1 will result in cells that have a defect in DNA replication. This was observed in cells depleted for RPA1 (Fig. 1*C*). The replication defect is not detectable until at least 72 h after siRNA introduction, and the maximal phenotype occurs between 96 and 120 post-transfection. This is consistent with a time when RPA1 levels are most reduced (Fig. 1*A*). The phenotype that is observed is a dramatic increase in the S phase population of cells (Figs. 1*C*, 2, *B–D*; Table 1). The percentage of S phase cells in the experiment shown in Fig. 1*C* increases from 27.2% in mock-transfected cells to 66.1% in RPA1-depleted cells (Table 1). The observed increase in S phase cells is presumably due to a replication defect, because the increase in S phase cells is concomitant with a decrease in G_1 phase cells from 62.5% in mock-transfected cells to 18.2% in RPA1 siRNA-transfected cells (Table 1). The accumulation of cells in S phase varies between individual experiments but ranges from 57 to 73%, whereas mock-transfected cells in S phase range from 18 to 32%. To examine the definitive phenotype when RPA1 is depleted, RPA1-depleted cells were synchronized with aphidicolin, an inhibitor of DNA polymerases (49), and subsequently released into aphidicolin-free media. These cells were found to arrest as a homogeneous population at the G_1/S boundary (data not shown). These results are consistent with RPA1 being essential for entry into S phase and suggest that S phase accumulation observed with asynchronous cells is a result of some cells partially progressing into S phase before sufficient depletion of RPA1 has occurred. Additionally, RPA1 knockdown results in a decrease in cell viability as indicated by an increase in sub-G_1 cells 96 h after introduction of siRNA (data not shown).

RPA1 depletion also results in a significant (Mann-Whitney test; $p = 0.0012$) increase in G_2/M cells (Table 1), suggesting that depletion of RPA1 is triggering a checkpoint arrest. To test this, RPA1-depleted cells were treated with caffeine, a potent inhibitor of the family of phosphatidylinositol 3-kinase (*e.g.* ATM, ATR, and DNA-PK) activity (50) necessary for checkpoint function, for 24 h prior to cell collection and analysis. Fig. 1*D* shows that the accumulation of cells in G_2/M is alleviated in the presence of caffeine, indicating that the accumulation of cells in G_2/M is a result of activation of the G_2/M checkpoint. We conclude that depletion of RPA1 results in the activation of the cellular G_2/M checkpoint, which is similar to the conclusion by Dodson *et al.* (14). In contrast, RPA1-depleted cells remain in S phase after caffeine treatment. This demonstrates that the accumulation of cells in S phase is caused by a deficiency in cellular DNA replication and is not exclusively the consequence of intra-S checkpoint activation (Fig. 1*D*). This confirms in human cells that RPA1 has an essential role in chromosomal DNA replication and is not merely a replication defect where cells proceed through S phase more slowly. This would also indicate that the inability to proceed through G_2/M is not directly attributable to a lack of RPA1 protein.

The RPA1 Knockdown Phenotype Can Be Rescued by Exogenous Expression of N-terminally GFP-tagged RPA1 but Not by Expression of Other RPA Subunits—To examine RPA1 function in the cell it is necessary to replace endogenous RPA1 with readily detectable exogenous forms of RPA1. We generated an N-terminally GFP-tagged form of RPA1. This construct does not contain the endogenous 3′-UTR region, and thus its expression is not targeted by the RPA1 siRNA. After siRNA introduction, but before manifestation of the knockdown phenotype ($t = 24$), a plasmid directing the expression of this exogenous RPA1 was introduced into the cells by transfection. Cells that contain the plasmid and are expressing the exogenous RPA (GFP-positive cells) can then be quantitated by flow cytometry. To gain insight into the level of exogenous GFP-RPA1 expression in each cell, we examined expression by immunoblotting (Fig. 2*A*) and flow cytometry (Fig. 2*B*).

Immunoblotting revealed that the intensity of exogenous GFP-RPA1 is on average 10–30% of the level of endogenous RPA1 observed for mock-transfected cells (Fig. 2*A*, compare *lane 4* with *lane 1*). Flow cytometry revealed that the GFP-RPA1 fusion protein on average is expressed in 10–30% of the cells collected at 96 h after knockdown (72 h after transfection of the GFP-RPA1 plasmid) (see *left side* of Fig. 2*B*). Because ~30% of the cells express the GFP-RPA1 fusion protein, and the total expression of GFP-RPA1 for the population of cells (both expressing and not expressing GFP-RPA1) is ~30%, this would indicate that GFP-RPA1 expression levels in the cell are similar to or slightly lower than endogenous RPA1 expression levels in mock-transfected cells at this time point. In all cases, we observed higher levels of the GFP-RPA1 fusion protein in extracts made from siRNA-treated cultures (Fig. 2*A*, compare *lane 4* with *lane 2*). We believe this is a result of cells lacking RPA1 being less viable and thus contributing less protein to these extracts.

When examined at 96 h after knockdown of endogenous RPA1, the cell cycle distribution of GFP-RPA1-containing cells

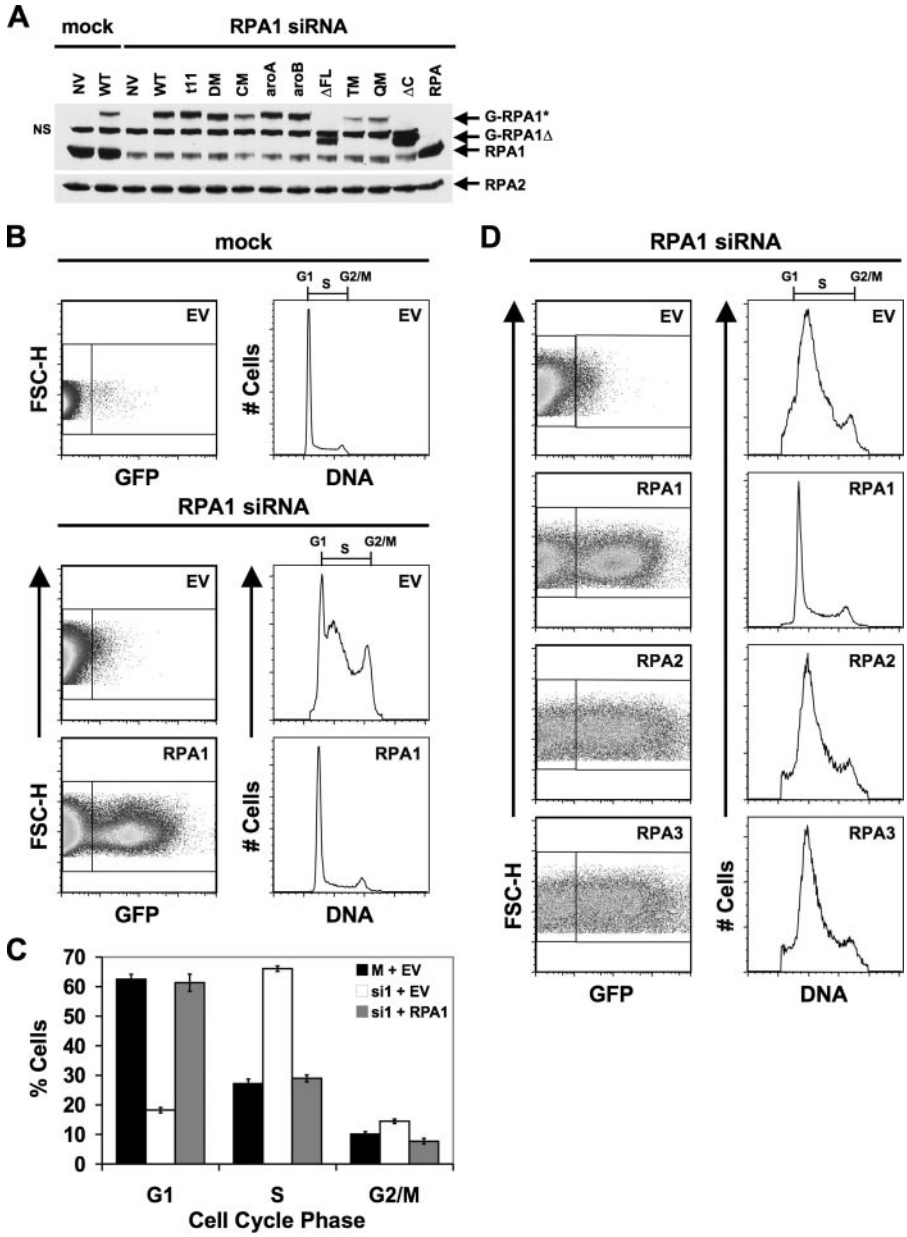

FIGURE 2. **Rescue of RPA1 knockdown by exogenous RPA1.** *A,* cells were either mock- or RPA1 siRNA-transfected. After 24 h, the cells were transfected with either exogenous GFP-tagged RPA1 vector (*WT*) or with various GFP-tagged RPA1 mutants (t11, DM, CM, aroA, aroB, ΔFL, TM, QM, and ΔC) denoted *above* each lane of the gel. Polyclonal N2.2 antibody was used to detect endogenous and exogenous GFP-tagged RPA1, as well as RPA2. *RPA*, 100 ng of purified recombinant human RPA; *NV*, no vector; *NS*, nonspecific band. *B,* expression of exogenous RPA1 after knockdown of endogenous RPA1. Cells were either mock- or RPA1 siRNA-transfected (designated *above* dot-plots and histograms). After 24 h, the cells were transfected with either an empty vector (*EV*) or exogenous GFP-tagged RPA1 vector (designated in the *upper right corner* of each dot-plot). At 96 h, cells were stained for flow cytometry, and exogenous RPA1-positive cells were identified based on their green (*GFP*) fluorescence (FL1-H, *left panels*). The DNA content of RPA1-positive cells (*right box* in dot-plot) was plotted as a histogram (*right panels*) as in Fig. 1*C* for all samples transfected with WT RPA1 vector. The DNA content of RPA1-negative cells (*left box* in dot-plot) was plotted for all samples transfected with an empty vector. *C,* quantitation of the percentage of cells from *B* in each stage of the cell cycle. *D,* expression and rescue by other RPA subunits after RPA1 knockdown. Cells were transfected as in *A*, except that 24 h after RPA1 siRNA transfection, cells were transfected with an empty vector, exogenous RPA1, exogenous RPA2, or exogenous RPA3. Samples are designated as in *A*. In this experiment, the RPA1 siRNA cell cycle defect (accumulation of cells in S phase, decrease of cells in G_1 phase) is more pronounced than in *A*, thus the G_1 peak is not readily detectable. The severity of the RPA1 knockdown phenotype shows some experimental variation; however, this range of phenotype is normal. Note that the defect is fully rescued by exogenous RPA1 expression.

was indistinguishable from cells that were mock-transfected or scrambled siRNA-transfected (Fig. 2, *B* and *C*; Table 1; data not shown). Rescue of the normal cell cycle distribution by exogenous RPA1 demonstrates that exogenous expression of GFP-RPA1 is sufficient to substitute for loss of endogenous RPA1. These results also show that the siRNA knockdown phenotype is specific for RPA1, and that the presence of an N-terminal GFP tag does not detectably disrupt RPA function.

To examine whether the rescue of the cell cycle phenotype is specific for exogenous RPA1, we attempted to complement RPA1 knockdown with N-terminally GFP-tagged RPA2 and RPA3. Each construct was introduced into cells 24 h after introduction of the RPA1 siRNA (prior to maximal RPA1 knockdown). Expression of either exogenous GFP-RPA2 or GFP-RPA3 could be readily detected after RPA1 knockdown as a population of GFP-positive cells (Fig. 2*D*). Although RPA2 or RPA3 were not targeted for degradation after RPA1 knockdown, exogenous expression of these subunits cannot rescue the RPA1 knockdown phenotype (Fig. 2*D*). This indicates that although the other RPA subunits are stable in the absence of RPA1, they cannot compensate for the loss of RPA1 in the cell.

Biochemical Characterization of RPA1 Mutants—To understand the roles of the individual domains of RPA1 in the cell, a series of mutant forms of RPA1 were made. The major ssDNA binding activity lies in the two central domains of RPA1 subunit: DBD-A and DBD-B (19). Domain mapping studies and NMR analysis have shown that of these two DNA-binding domains, DBD-A has the highest affinity for ssDNA (17, 18, 51). X-ray crystallographic analysis of RPA1 DBD-A and DBD-B has allowed for identification of residues in these domains that interact with an eight nucleotide oligodeoxycytosine (dC_8) (52). The RPA-ssDNA interface consists of both polar interactions and nonpolar base-stacking interactions (52). To understand the contribution of the interacting residues to ssDNA binding affinity, RPA heterotrimers containing mutations in DBD-A or DBD-B were generated and purified.

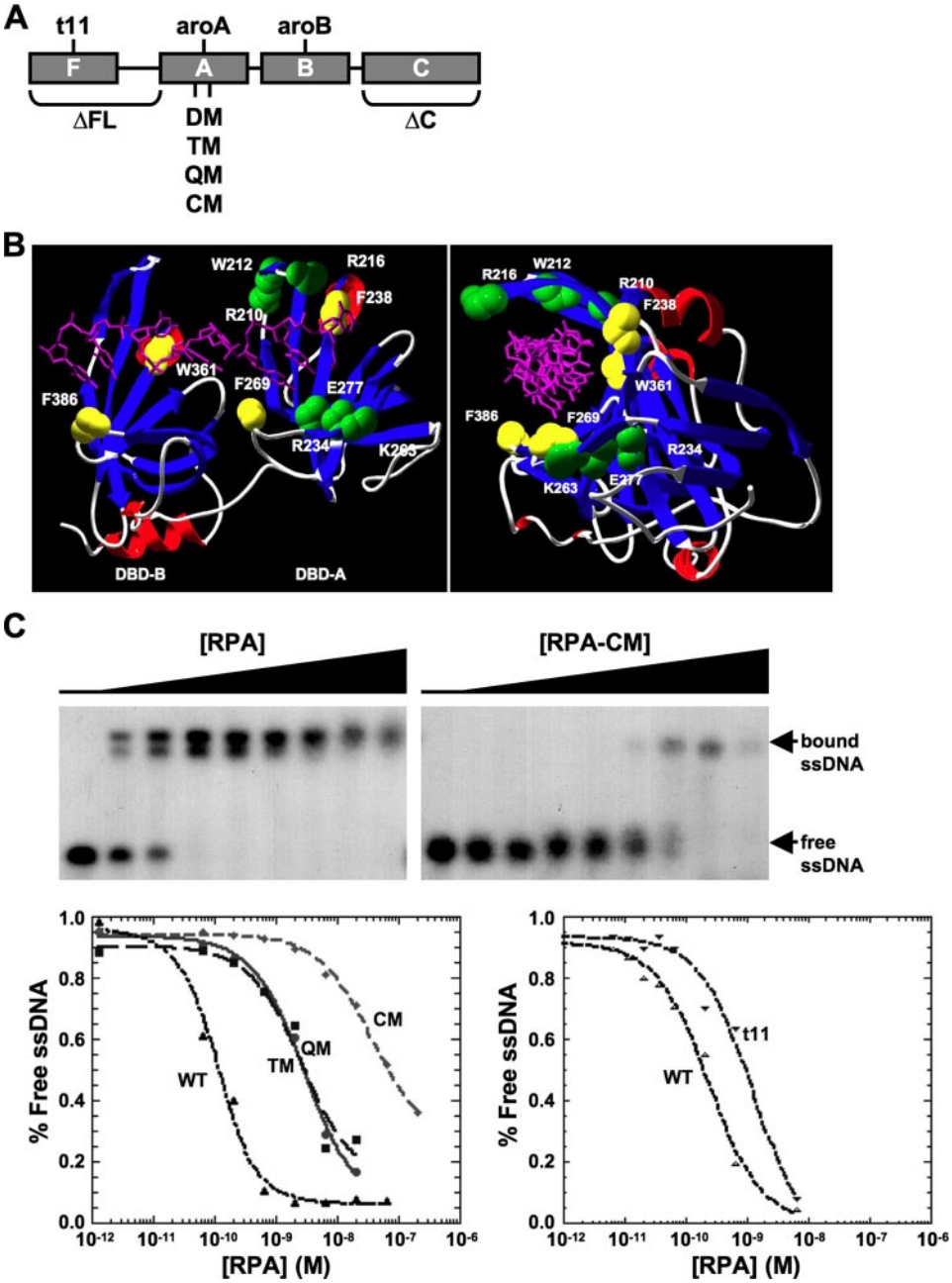

FIGURE 3. **Mutations in RPA1 DNA and purification of mutant RPA.** *A,* schematic showing the domain organization of RPA1. The OB-folds, referred to as DBDs, are designated as DBD-F, DBD-A, DBD-B, and DBD-C for RPA1. The extended linker region between DBD-F and DBD-A is designated by a *horizontal line*. Each mutation used in these studies is labeled, and the approximate location of each mutation examined is shown. *B,* locations of mutations in residues that interact with DNA are depicted on crystal structure (52) of DBD-A and DBD-B. Polar residues (*green*), aromatic residues (*yellow*), and dC_8 (*purple*) are shown. The *letter* depicts the amino acid, and the *number* represents its position in RPA1. *Left* and *right panels* are front and right-side views of the structure, respectively. *C,* ssDNA binding affinity analysis of RPA1 DBD-A mutants by electrophoretic mobility shift assay (*EMSA*). Gels are shown for WT RPA (*left*) and RPA1-CM (*right*) binding to $(dT)_{30}$. The positions of free and bound ssDNA are denoted to the *right* of the gels. The concentration of RPA used is qualitatively shown above each gel (height of increase is relative among all gels). The *bottom* of the figure shows representative binding curves for RPA1 DBD-A polar-interacting mutants (*bottom left*) and RPA1-t11 (*bottom right*). See Table 2 for summary of binding data.

Previous biochemical analyses showed that mutation of polar-interacting residues (shown in *green* in Fig. 3*B*) in the DNA-binding site of DBD-A causes a dramatic reduction in ssDNA binding of the entire RPA complex (17). For example, mutation of two polar-interacting residues to alanine, K263A and E277A (RPA1-DM), resulted in an RPA complex with an affinity for ssDNA that was less than 1% of wild-type (WT) RPA (K_a = $3.0 \times 10^8\ M^{-1}$ *versus* $360 \times 10^8\ M^{-1}$ for WT; Table 2; and Wyka *et al.* (17)). To further explore the role of RPA-ssDNA binding through polar interactions, additional mutations were made in DBD-A to generate a series of mutant forms with three (RPA1-TM), four (RPA1-QM), and six (RPA1-CM) polar-interacting residues mutated to alanine. In each case, the mutant RPA1 was expressed along with the other two RPA subunits in *Escherichia coli,* and the mutant complexes were purified. All three mutants expressed at levels similar to WT RPA and were purified to homogeneity (data not shown). The yields of RPA1-TM and RPA1-QM complexes were similar to WT RPA, whereas purification of the RPA1-CM complex consistently resulted in a lower yield of protein (data not shown). We conclude that the recombinant RPA1-CM complex is less stable during purification than the other mutant complexes. The ssDNA binding activity of each form was determined in electrophoretic mobility shift assays. The two RPA mutants that had three or four polar residues in the DNA-binding site mutated, RPA1-TM (R234A, K263A, and E277A) and RPA1-QM (R216A, R234A, K263A, and E277A), were found to have an affinity for ssDNA similar to RPA1-DM (Table 2). The RPA1-CM complex, in which all of the polar residues in DBD-A that interact with dC_8 were mutated to alanine residues (R210A, W212A, R216A, R234A, K263A, and E277A) showed a further reduction in ssDNA binding; the mutant complex was reduced ($K_a = 0.28 \times 10^8\ M^{-1}$) to less than 0.1% of WT RPA (Fig. 3*C*; Table 2).

In addition to polar interactions with DNA, there are also four aromatic residues (two in DBD-A and two in DBD-B; shown in *yellow* in Fig. 3*B*) identified to be involved in nonpolar base-stacking interactions with dC_8 (52). Mutation of the interacting aromatic residues in DBD-A (RPA1-aroA; F238A and F269A) or in DBD B (RPA1-aroB; W361A and F382A) in human RPA has been shown to reduce ssDNA binding to 23 and 14% of WT

TABLE 2
ssDNA binding affinities of RPA1 mutants

RPA mutant[a]	Location of mutation(s) or deletion	Mutation(s)	$(dT)_{30}$ binding affinity ($K_a(\times 10^8\ M^{-1})$)	Relative binding affinity
				%
WT			360 ± 230	100
RPA1-DM[b,c]	DBD-A	K263A E277A	3.0 ± 0.6[b]	0.84
RPA1-TM[c]	DBD-A	R234A K263A E277A	3.2 ± 0.3	0.89
RPA1-QM[c]	DBD-A	R216A R234A K263A E277A	3.5 ± 0.6	0.97
RPA1-CM[c]	DBD-A	R210A W212A R216A R234A K263A E277A	0.28 ± 0.15	0.08
RPA1-aroA[b,d]	DBD-A	F238A F269A	82 ± 8.6[b]	23
RPA1-aroB[b]	DBD-B	W361A F386A	52 ± 8.6[b]	14
RPA1-t11	DBD-F	R41E Y42F	140 ± 5	38
RPA1-ΔFL[e]	DBD-F	Δ1–168	280 ± 200[e]	75
RPA1-ΔC[e]	DBD-C	Δ442–616	20 ± 15[e]	5

[a] Each RPA1 mutant examined was in the context of the heterotrimer.
[b] Data were from Wyka *et al.* (17).
[c] All mutants containing E277A also contain a conservative N281K substitution.
[d] The RPA1-aroA also contains a conservative S270T substitution.
[e] Data from Gomes and Wold (46) were normalized to the WT RPA examined in these studies.

RPA, respectively (17). These reductions in ssDNA binding are much less than that observed for mutations in polar-interacting residues.

In contrast to mutations of polar-interacting residues in the high affinity core of RPA, mutations in or deletions of the N terminus (DBD-F and linker) and the C terminus (DBD-C) do not lead to large changes in ssDNA binding (Table 2; Gomes and Wold (46)). Despite this, deletion of either the N terminus or C terminus of the yeast RPA1 homolog is lethal (28). Additionally, the *rfa1-t11* point mutation in the RPA1 gene in yeast leads to defects in DNA repair, recombination, and cell cycle regulation but not DNA replication (20, 31–33, 35). To examine the contribution of these domains to RPA1 function in human cells, we generated a mutation in the N terminus of RPA1 (RPA1-t11; R41E and Y42F) analogous to *rfa1-t11* in yeast, a deletion of the N terminus (RPA1-ΔFL; deletion of DBD-F and linker), and a deletion of the C terminus (DBD-ΔC; deletion of DBD-C) (Fig. 3*A*; Table 2). RPA1-ΔFL (originally called RPA70·ΔN168) and RPA1-ΔC (originally called RPA70·ΔC442) have been purified and characterized previously (23, 46), and both have high affinity ssDNA binding. RPA1-ΔFL has WT RPA ssDNA binding affinity, and RPA1-ΔC has an affinity ~5% of WT RPA affinity (23, 46). In the case of RPA1-ΔC, the subunit interaction domain (DBD-C) of RPA1 has been deleted, and the protein purifies as a single soluble polypeptide without RPA2 and RPA3 (23, 46). The RPA heterotrimer containing RPA1-t11 was highly expressed in *E. coli* and purified in high yield (data not shown). The RPA complex containing RPA1-t11 also had high affinity binding for ssDNA ($K_a = 140 \times 10^8\ M^{-1}$; Fig. 3*C*; Table 2), similar to findings for Rfa1-t11 in yeast (32). These data demonstrate that forms of RPA with a deletion of either terminus or the t11 mutation (R41E, Y42F) in DBD-F are stable *in vitro* and have high affinity ssDNA binding activity.

Rescue of RPA1 Knockdown Phenotype by Exogenous RPA1 Mutants—From the data obtained for ssDNA binding, it is clear that mutations in DBD-A and DBD-B can drastically affect ssDNA binding, whereas a mutation in or a deletion of DBD-F or DBD-C has a smaller negative effect on RPA affinity for ssDNA. We next carried out knockdown and replacement studies to determine the contributions of each domain and ssDNA binding affinity to the function of RPA in the cell. Each mutant form of RPA1 was expressed as a GFP fusion protein in HeLa cells in which endogenous RPA1 had been removed by siRNA transfection.

GFP-RPA1-DM was expressed at levels similar to WT GFP-RPA1 based on immunoblotting (compare Fig. 2*A*, *lane 6* with *lane 4*) and levels of green fluorescence intensity detected by flow cytometry (compare *left panels* of Figs. 2*B* and 4*A*). In addition, in each experiment the fraction of cells expressing GFP-RPA1-DM is similar to that observed expressing WT GFP-RPA1. RPA1-depleted cells expressing RPA1-DM had a cell cycle distribution that was indistinguishable from that of WT RPA1 (compare Fig. 4*A* and *B,* with 2, *B* and *C*). We conclude that RPA1-DM, which has a binding affinity less than 1% of WT RPA, can rescue the replication defect observed in RPA1 knockdown cells.

We also tested GFP fusions of RPA1-TM and RPA1-QM. These mutants contain additional mutations in DBD-A but have an affinity for ssDNA similar to RPA1-DM. These fusion proteins were expressed as full-length polypeptides based on immunoblot analysis but were detected at lower levels than WT GFP-RPA1 or GFP-RPA1-DM (Fig. 2*A*). Quantitation of the fluorescence intensity of GFP-positive cells by flow cytometry (an indicator of the per cell level of protein expression) indicated that the intensity of the GFP fluorescence of those cells was similar to WT GFP-RPA1 (data not shown). Thus, it is most likely that the reduced protein level observed in immunoblot analysis is a product of fewer cells in the culture expressing the RPA construct. Consistent with this, there is always a strong correlation between the proportion of GFP-positive cells examined by flow cytometry and the amount of GFP-tagged mutant RPA1 protein detected by immunoblotting (data not shown). When the cell cycle distribution of cells expressing GFP-RPA1-TM and GFP-RPA1-QM was examined, the distribution was similar to mock-depleted or WT GFP-RPA1-expressing cells (compare Fig. 4, *A* and *B* with Fig. 2, *B* and *C*). These results support the conclusion that RPA1 forms with significantly reduced ssDNA binding activity can support normal DNA replication. These results also indicate that although RPA1-TM and RPA1-QM protein levels are reduced, they can still function in the cell.

RPA1-CM contains six mutations (R210A, W212A, R216A, R234A, K263A, and E277A), eliminating all of the polar interactions between DBD-A and ssDNA observed in the crystal structure. In contrast to RPA1-DM, RPA1-TM, and RPA1-QM, RPA1-depleted cells expressing RPA1-CM showed a cell cycle distribution similar to that of RPA1 knockdown cells (Fig. 4, *A* and *B*). GFP-RPA1-CM was expressed as a full-length protein and appeared to be present in the cultures at levels comparable

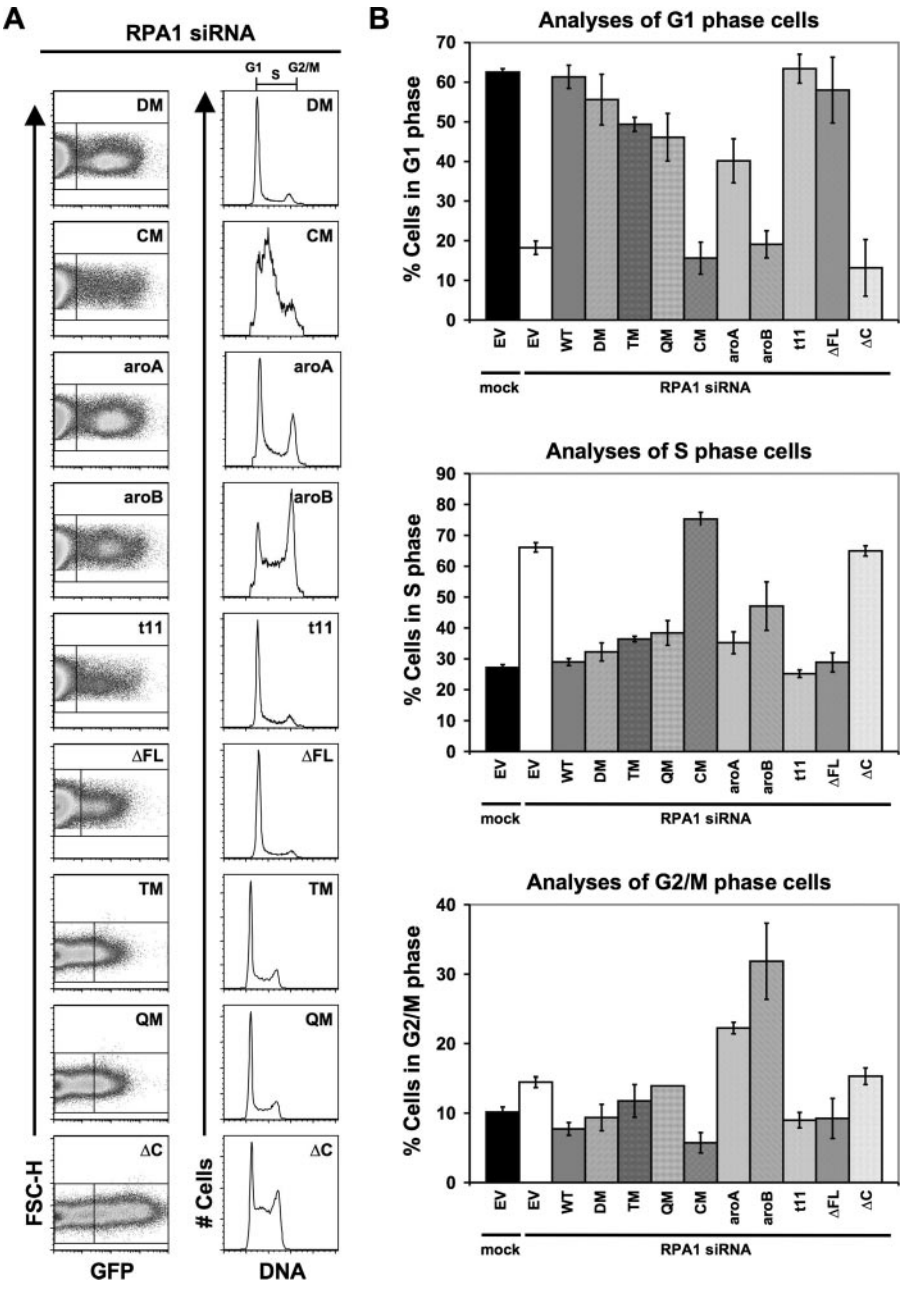

FIGURE 4. **Differential effects on DNA replication and cell cycle progression by RPA1 mutants.** *A,* complementation of RPA1 knockdown by RPA1 and RPA1 mutants (designated in *upper right corner* of each dot-plot and histogram as *DM, CM, aroA, aroB, t11,* ΔFL, TM, OM, and ΔC) is shown. Cells were treated and examined, and all designations are as described in Fig. 2*B*. *B,* graphical representation of the distribution of cells from *A*, in G_1 (*top*), S (middle), and G_2/M (*bottom*) phases of the cell cycle.

with or even greater than those of RPA1-TM and RPA1-QM (slightly lower levels than WT RPA1; Fig. 2*A*). Cells expressing RPA1-CM had similar GFP fluorescence intensity (an indicator of level of protein expression) to cells expressing other RPA1 forms (Fig. 4*A*); however, consistently fewer GFP-positive cells were observed in cultures with GFP-RPA1-CM than with WT GFP-RPA1. This can be explained if one presumes that loss of RPA1 activity results in death of the cell, which would result in a consistently lower number of GFP-positive cells for a non-functional mutant. Taken together, these data indicate that per cell expression levels of GFP-RPA1-CM are at least equivalent to those of GFP-RPA1-TM and GFP-RPA1-QM and may approach that of WT RPA1. Because RPA1-TM and RPA1-QM reconstitute normal cellular functions, we conclude that the inability of RPA1-CM to function is more likely to be due to a reduction of activity (*i.e.* reduced ssDNA binding to 0.1% of WT RPA) rather than reduced expression.

We also examined the role of aromatic residues in DBD-A and DBD-B in cellular function. RPA1-aroA and RPA1-aroB have mutated pairs of ssDNA-interacting aromatic residues in DBD-A or DBD-B, respectively (Fig. 3, *A* and *B*). Both of these proteins were expressed as full-length GFP fusions at levels comparable with WT RPA1 (Figs. 2*A* and 4*A*). When RPA1-aroA and RPA1-aroB were exogenously expressed in cells depleted for endogenous RPA1, two distinct phenotypes were observed (Fig. 4*A*). First, both mutants display a dramatic reduction in S phase cells (RPA1-aroA = 35%; RPA1-aroB = 47%) compared with RPA1-depleted cells (66%) (Fig. 4*A* and *middle panel* of *B*). This suggests that both mutants are able to support a substantial amount of DNA replication (Fig. 4, *A* and *B*; Table 1). The second phenotype observed in cells expressing RPA1-aroA and RPA1-aroB is an accumulation of cells in G_2/M phase (RPA1-aroA = 22% and RPA1-aroB = 32% *versus* WT RPA1 = 8%), suggesting there is a cell cycle defect with these forms of RPA (Fig. 4, *A* and *C*; Table 1; Fig. 5). To test whether the G_2/M accumulation was an arrest caused by checkpoint activation or the result of a defect in mitosis, the cells were treated with caffeine. This treatment effectively eliminates the accumulation of cells in G_2/M, indicating that RPA1-aroA and RPA1-aroB are triggering a checkpoint involving the family of phosphatidylinositol 3-kinase activity (Fig. 5*C*). Given that the replication defect is not completely rescued (as indicated by cells remaining in S phase), it is possible that the replication occurring in RPA1-aroA and RPA1-aroB mutants is imperfect and results in checkpoint activation.

A number of mutations have been identified in the N-terminal domain of *S. cerevisiae* RPA1 (*RFA1*) that cause UV and methyl methanesulfonate sensitivity (20). One mutation that has been extensively studied is *rfa1-t11*, which is functional for

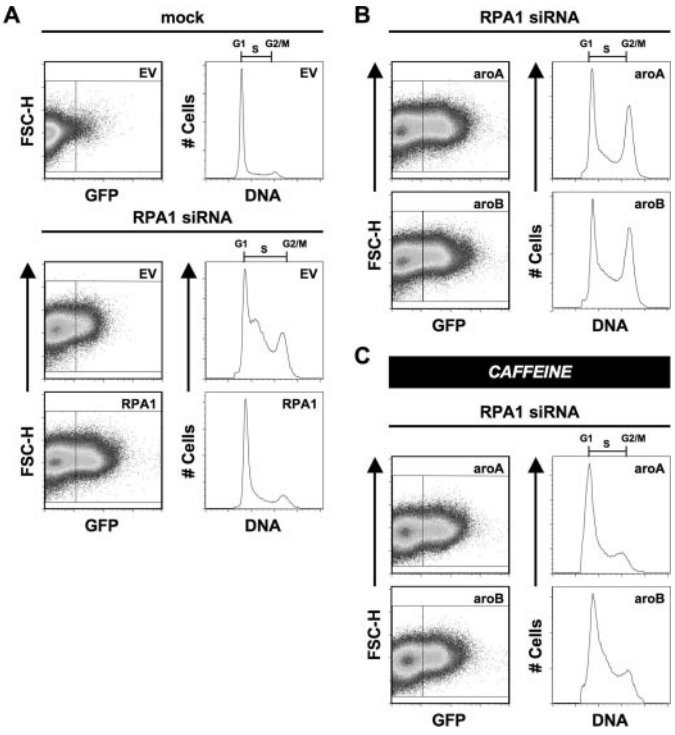

FIGURE 5. **Examination of RPA1-aroA and RPA1-aroB mutants.** *A*, expression of exogenous RPA1 after knockdown of endogenous RPA1. Cells were either mock- or RPA1 siRNA-transfected (designated *above* dot-plots and histograms). After 24 h, the cells were transfected with either an empty vector (*EV*) or exogenous GFP-tagged RPA1 vector (designated in the *upper right corner* of each dot-plot). At 96 h, cells were stained for flow cytometry, and exogenous RPA1-positive cells were identified based on their green fluorescence (FL1-H). The DNA content of RPA1-positive cells (*right box*) was plotted as a histogram. The DNA content of RPA1-negative cells (*left box*) was plotted for all samples transfected with empty vector. *B*, phenotypes of RPA1-depleted cells containing exogenously expressed RPA1-aroA and RPA1-aroB. Cells were treated and examined, and all designations are as described in Fig. 2*B*. *C*, phenotypes of RPA1-depleted cells containing exogenously expressed RPA1-aroA and RPA1-aroB after 3 mM caffeine treatment. Cells were treated and examined, and all designations are as described in Fig. 2*B*.

DNA replication and cell viability (20) but is defective in recombination and cell cycle regulation after DNA damage (13, 32). The analogous mutation in human RPA1 shows near wild-type ssDNA binding affinity (Fig. 3*D*; Table 2). When we tested the function of human RPA1-t11, we found that it was able to completely rescue the replication defect observed after RPA1 knockdown (Fig. 4, *A* and *B*; Table 1). This is consistent with both yeast mutant data and the high affinity for ssDNA for human RPA1-t11.

The N-terminal domain of RPA1 (DBD-F) can interact with ssDNA, with multiple proteins, and has been suggested to play a role in regulating RPA function upon phosphorylation of RPA2 (22, 53). To examine the importance of this domain in human cells, we tested whether an RPA1 mutant with the first 168 amino acids removed (RPA1-ΔFL) could complement RPA1 deficiency. In yeast, it had been shown that DBD-F is important for cellular function, because if more than 10 amino acids are deleted from the N terminus of *RFA1*, the cells are not viable (28). Surprisingly, expression of RPA1-ΔFL results in a cell cycle distribution that is indistinguishable from wild-type RPA1 (Fig. 4, *A* and *B*; Table 1). We conclude that DBD-F and the linker region between DBD-F and DBD-A are dispensable for DNA replication in human cells.

Deletion of DBD-C (RPA1-ΔC) slightly decreases the affinity of RPA for ssDNA; however, this form of RPA1 is incapable of forming a heterotrimeric complex with RPA2 and RPA3 (23). When examined in unstressed RPA1-depleted cells, RPA1-ΔC could not rescue the replication defect (Fig. 4), consistent with previous results examining SV40 replication *in vitro* (23). RPA1-ΔC is not functional, despite having a high affinity for ssDNA (binding is similar to RPA1-aroA, RPA1-aroB, and RPA1-t11). This demonstrates that the C termini of RPA1 and/or RPA2/RPA3 are necessary for RPA function in the cell.

Localization of RPA1 Mutants to Sites of DNA Damage—After DNA damage, RPA colocalizes at distinct foci with other proteins required for DNA repair in human cells (54). We next determined what activities of RPA1 are necessary for RPA localization. Following endogenous RPA1 knockdown and exogenous expression of different forms of RPA1, cells were treated with DNA-damaging agents. CPT is a topoisomerase I inhibitor that causes single strand breaks (55–57) and causes either endogenous RPA1 or exogenous GFP-RPA1 to localize to foci (Fig. 6*A*). When RPA1 containing mutations of ssDNA-interacting polar residues in DBD-A were examined, it was observed that RPA1-DM, RPA1-TM, and RPA1-QM are also found at sites of DNA damage (Fig. 6*B*). This is consistent with these mutant forms appearing to function like WT RPA1 and indicates that the ssDNA binding activity retained in RPA1-DM, RPA1-TM, and RPA1-QM (~1% wild-type) is sufficient for normal localization after DNA damage.

Localization of RPA1-CM was also examined after CPT treatment. No foci were observed in RPA1-CM mutant cells. Although we cannot completely rule out protein stability or altered cellular localization as the culprit, the expression analysis described previously strongly suggest that the lack of RPA1-CM foci is because of altered ssDNA binding (Fig. 2; data not shown).

When the aromatic mutants were examined, we were surprised to observe that despite having higher ssDNA binding affinity than RPA1-DM, localization of RPA1-aroA and RPA1-aroB to DNA repair foci could not be detected after CPT treatment (Fig. 6*B*). The ability of the different forms of RPA1 to support foci formation were similar (data not shown) when cells were treated with the topoisomerase II inhibitor ETP (58).

As mentioned above, DBD-F of yeast RPA1 appears to have a substantial role in the DNA damage response. We therefore determined whether the DBD-F mutants could localize to DNA damage foci. Both RPA1-t11 and RPA1-ΔFL were found as punctate foci after treatment with CPT (Fig. 6*C*) or ETP (data not shown) for 4 h. We conclude that any defect in DNA repair that is observed for DBD-F mutants is not because of an inability to recognize and bind DNA at sites of DNA damage. Interestingly, in yeast, Rfa1-t11 is also able to bind at damaged DNA sites (34). We conclude that the entire N terminus of RPA1 (DBD-F and the linker) is dispensable for localization to sites of DNA repair after damage (Fig. 6*C*) and that any defect in repair is downstream of localization.

The histone variant, H2AX, becomes phosphorylated when DNA damage is present in cells (59). H2AX phosphorylation

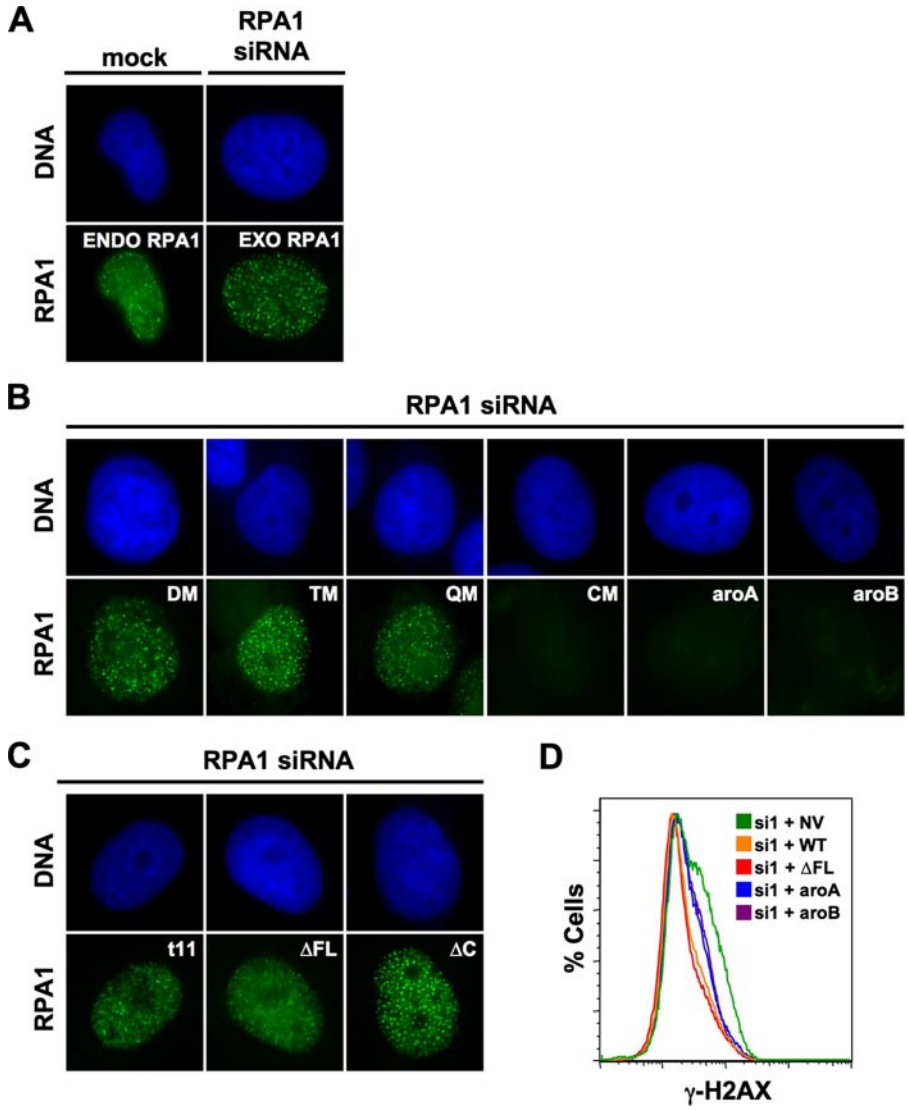

FIGURE 6. **Localization of RPA1 mutants to sites of DNA damage.** *A*, localization of RPA1 to sites of DNA damage. At 96 h after mock transfection (*left side*) or post-transfection of RPA1 siRNA (*right side*), cells were treated with 2 μM CPT for 4 h prior to fluorescence microscopy analysis. *Top row* shows nucleus (DAPI staining); *bottom row* shows RPA1. Endogenous (*ENDO*) RPA1 was detected in mock-transfected cells with α-RPA1 (2H10). Exogenous (*EXO*) GFP-RPA1 was detected in endogenous RPA1-depleted cells using GFP fluorescence. *B*, localization of RPA1 DBD-A and DBD-B mutants to DNA damage foci. At 96 h post-transfection of RPA1 siRNA (and transfection of exogenous GFP-tagged RPA1 mutant constructs), cells were treated as in *A*. Exogenous RPA1-DM (*DM*), RPA1-TM (*TM*), RPA1-QM (*QM*), RPA1-CM (*CM*), RPA1-aroA (*aroA*), and RPA1-aroB (*aroB*) are denoted in the *upper right corner* of the appropriate pair of panels. *C*, localization of RPA1 DBD-F and DBD-C mutants to sites of DNA damage. Exogenous RPA1-t11, RPA1-ΔFL, and RPA1-ΔC are designated in *upper right corner* of the appropriate panel pair. Cells were treated as described in *A*. *D*, detection of DNA damage in otherwise unstressed cells. Cells were collected at 96 h post-transfection of RPA1 siRNA and stained with γ-H2AX (Ser-139) antibody. Cells examined had no vector (*green line*), exogenous RPA1 (*WT*; *orange line*), RPA1-ΔFL (*ΔFL*; *red line*), RPA1-aroA (*aroA*; *blue line*), or RPA1-aroB (*aroB*; *purple line*). γ-H2AX staining is plotted as the percentage of cells (*% Cells*) *versus* FL4-H (*γ-H2AX*) fluorescence intensity. *si*, RPA1 siRNA; *NV*, no vector.

(γ-H2AX) is commonly used as a marker for the presence of DNA damage in the cell. To examine basal levels of DNA damage in cells when mutant forms of RPA1 are expressed, H2AX phosphorylation was quantitated. As shown previously (14), cells depleted of RPA1 had elevated phosphorylated γ-H2AX levels compared with cells that had been depleted and reconstituted with wild type RPA1 (Fig. 6*D*). Both RPA1-aroA and RPA1-aroB containing cells also had elevated γ-H2AX, suggesting that these mutant forms have defects in function that lead to elevated DNA damage in the absence of any exogenous DNA-damaging agents (Fig. 6*D*). RPA1-ΔFL containing cells showed no increase in γ-H2AX staining (Fig. 6*D*). We conclude that RPA1-ΔFL is capable of maintaining genomic DNA in an undamaged state in unperturbed cells.

Deletion of DBD-C (RPA1-ΔC) slightly decreases the affinity of RPA for ssDNA and prevents formation of a heterotrimeric complex with RPA2 and RPA3 (23). Despite this, RPA1-ΔC is capable of forming DNA damage foci (Fig. 6*C*). This demonstrates that RPA2 and RPA3 are not needed for RPA localization after DNA damage (presumably because of the high ssDNA binding affinity for RPA1-ΔC) but are needed for other RPA functions (*e.g.* replication and most likely subsequent steps of DNA repair).

The Role of RPA1 in Checkpoint Establishment/Maintenance after DNA Damage—In the experiments discussed above, high doses of DNA-damaging agent were used to allow for efficient RPA1 foci formation. We have also observed that treatment of HeLa cells with a medium dose of ETP (4 μM) or CTP (0.1 μM) for an extended period of time (48 h) results in the arrest of cells in the G_2/M phase of the cell cycle (Fig. 7*A*). This is because of activation of the G_2/M checkpoint by the presence of DNA damage. Cells depleted of RPA1 do not show as distinctive a G_2/M arrest; rather, there are a substantial number of cells that accumulate in S phase in addition to the accumulation of cells at the G_2/M boundary (Fig. 7*A*). This is consistent with depletion of RPA1 causing a defect in DNA replication. As with other RPA1 knockdown phenotypes, expression of exogenous WT RPA1 alleviates this defect (Fig. 7*A*). These data are consistent with exogenous RPA1 being able to function normally in DNA replication and in checkpoint activation after DNA damage.

When mutations in DBD-A and DBD-B were examined for the ability to support checkpoint function, it was found that the polar mutants reiterate the phenotype observed for untreated RPA1-depleted cells. RPA1-DM restores the G_2/M checkpoint, whereas RPA1-CM results in a distribution of cells similar to the RPA1-depleted cells (Fig. 7*B*). The aromatic mutations (RPA1-aroA and RPA1-aroB) also show phenotypes consistent

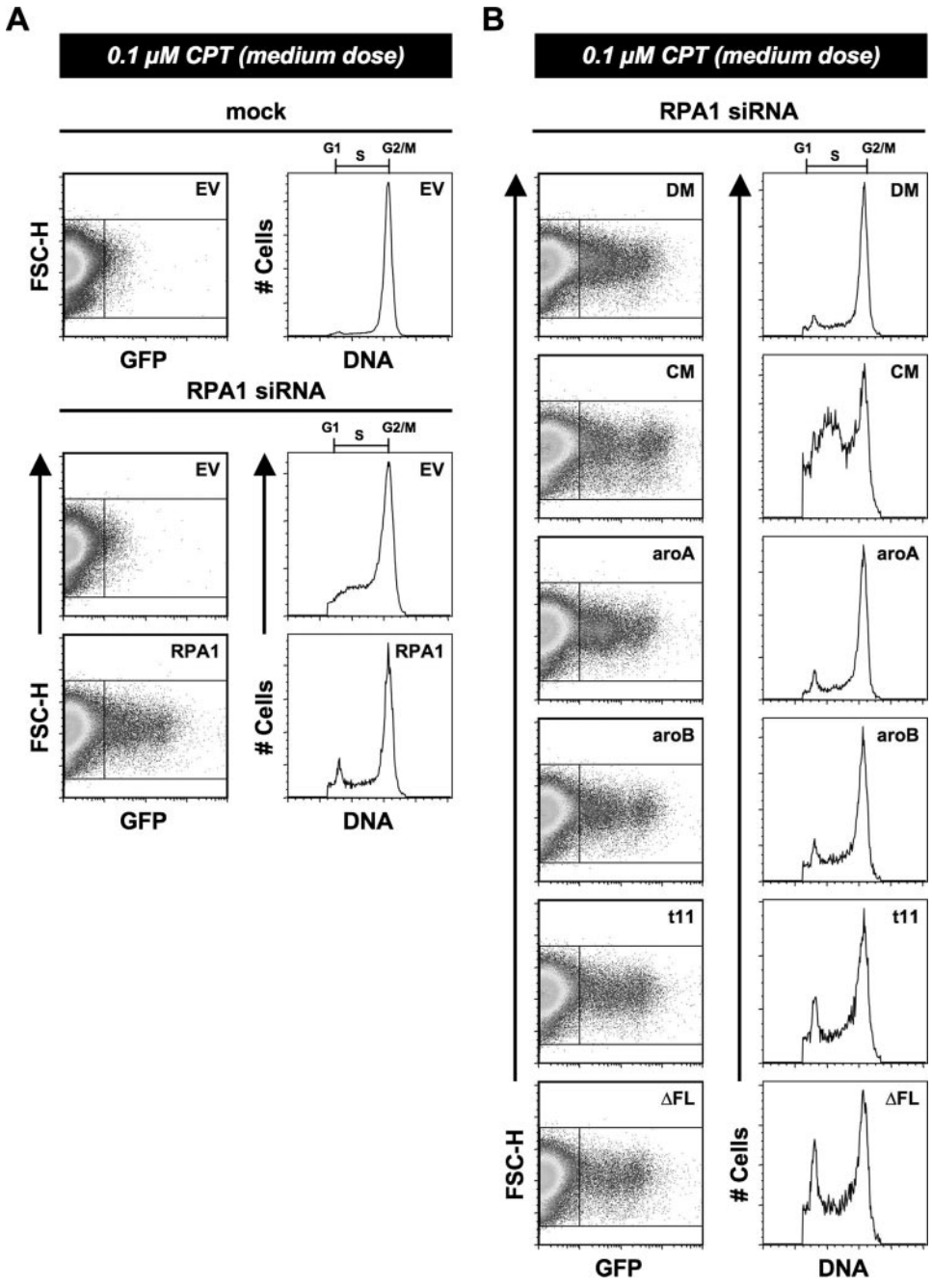

FIGURE 7. **RPA1 mutants and establishment of DNA damage-induced G_2/M arrest.** *A*, cells were either mock- or RPA1 siRNA-transfected (designated *above* each dot-plot and histogram). After 24 h, the cells were transfected with either empty vector (*EV*) or exogenous RPA1 vector (designated in the *upper right corner* of each dot-plot). At 48 h post-transfection of siRNA, the cells were treated with 0.1 μM CPT for 48 h. At 96 h, cells were stained for flow cytometry, and exogenous RPA1-positive cells were identified based on their green (GFP) fluorescence (FL1-H). The DNA content of RPA1-positive cells (*right box*) was plotted as a histogram as in Fig. 2*B* for all samples transfected with RPA1 vector. The DNA content of RPA1-negative cells (*left box*) was plotted for all samples transfected with empty vector as in Fig. 2*B*. *B*, establishment of G_2/M arrest after RPA1 knockdown by DBD-A and DBD-B mutants. Each mutant is designated in the *upper right corner* of each dot-plot and histogram as RPA1-DM (*DM*), RPA1-CM (*CM*), RPA1-aroA (*aroA*), RPA1-aroB (*aroB*), RPA1-t11 (*t11*), and RPA1-ΔFL. Cells were treated as in *A*, and examined as in Fig. 2*B*. All designations are as described in Fig. 2*B*.

with their phenotypes in undamaged cells. Both mutants have minimal number of cells in G_1 or S phase and have a majority of the cells accumulated in G_2/M (Fig. 7*B*) after DNA damage. We conclude that cells containing these mutants are able to successfully establish the G_2/M checkpoint in the presence of significant DNA damage.

rfa1-t11 is reported to be defective for the G_2/M checkpoint in yeast (13). Furthermore, this mutant shows the ability for adaptation in otherwise adaptation-deficient cells and appears to adapt better than *RFA1* cells (30, 35). Consistent with this, RPA1-t11 cells do not accumulate exclusively in G_2/M; rather, more cells appear in G_1 phase and throughout S phase than for WT RPA1 after a medium dose of CPT (Fig. 7*C*) or ETP (data not shown). RPA1-ΔFL cells show a similar phenotype to RPA1-t11 cells (Fig. 7*C*), suggesting that the function of DBD-F may lie strictly in cell cycle regulation and DNA repair.

An interesting phenomenon was observed when attempting to optimize the amount of CPT or ETP treatment that would lead to G_2/M arrest but prevent excessive cell death. When cells were treated with 10-fold less (low dose) CPT (0.01 μM) or ETP (0.4 μM), mock-transfected or WT RPA1-transfected (after RPA1 knockdown) cells show little or no discernible cell cycle phenotype (Fig. 8*A*). At this same low dose of CPT or ETP, RPA1-t11 and RPA1-ΔFL cells show an increase in G_2/M cells (Fig. 8). Both RPA1-t11 and RPA1-ΔFL can support G_2/M checkpoint activation (Figs. 7 and 8). So any G_2/M defects observed for these mutants are probably not because of a defect in establishing the G_2/M checkpoint. In addition, in the absence of DNA-damaging agents, there was no increase in γ-H2AX in cells reconstituted with RPA1-ΔFL (Fig. 6*D*), indicating that basal DNA damage is not elevated in these cells. Therefore, it is most likely that the increased checkpoint activation observed with low doses of damage is the result of a deficiency in DNA repair. These findings are similar to those for Rfa1-t11 in yeast, and suggest a role for the N-terminal domain of RPA1 that may lie exclusively in the response to DNA damage.

DISCUSSION

RPA is essential for multiple processes in DNA metabolism. This has made it a challenge to dissect its various func-

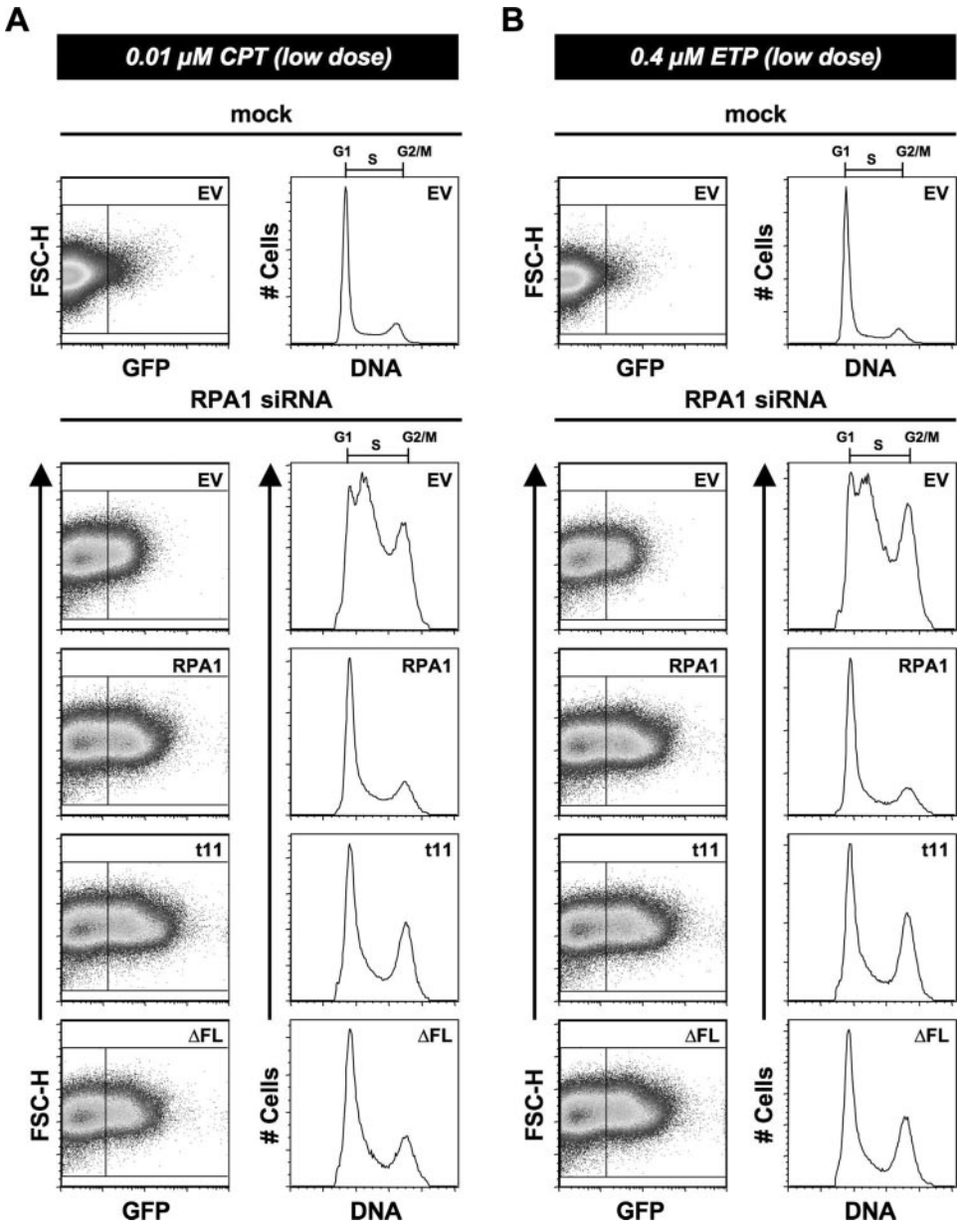

FIGURE 8. **Examination of DBD-F mutants under conditions of lower chemically induced DNA damage.** *A,* cells were either mock- or RPA1 siRNA-transfected (designated *above* each dot-plot and histogram). After 24 h, the cells were transfected with either empty vector (*EV*) or exogenous RPA1 vector (designated in the *upper left corner* of each dot-plot). At 48 h post-transfection of siRNA, the cells were treated with 0.01 μM CPT for 48 h. At 96 h, cells were stained for flow cytometry, and exogenous RPA1-positive cells were identified based on their green (GFP) fluorescence (FL1-H). The DNA content of RPA1-positive cells (*right box*) was plotted as a histogram as in Fig. 2*B* for all samples transfected with RPA1 vector. The DNA content of RPA1-negative cells (*left box*) was plotted for all samples transfected with empty vector as in Fig. 2*A*. *B*, cells were treated and examined as in Fig. 8*A*; however, these cells were treated with 0.4 μM ETP for 48 h.

tions *in vivo*. To address this issue and to define the functions of the domains of RPA1 *in vivo*, we have utilized RNAi to deplete endogenous RPA1 levels and then introduced exogenous forms of RPA by transient transfection. This has led to a number of insights into the function of RPA in the cell.

The Effects of RPA1 Depletion on the Cell—RPA exists as a very stable heterotrimeric complex *in vitro* (10, 45). In addition, a subcomplex containing RPA2 and RPA3 forms *in vitro* and is stable in solution (27, 45, 60). Our Western and flow cytometric analyses demonstrate that RPA1 depletion does not affect the stability of RPA2 under the conditions used in our studies, similar to previous reports (14, 40). Flow cytometric analysis and immunoblotting (data not shown) also indicate that RPA3 is unaffected after RPA1 knockdown. This suggests that the subcomplex of RPA2 and RPA3 can form and is stable in human cells. It has been reported that the RPA subunits are localized to different regions of the cell after S phase (61). Although the RPA heterotrimer appears to be stable in cells (62), it is possible that differential localization of RPA1, RPA2, and RPA3 could also could be due to the presence of RPA2 and RPA3 subcomplexes in the cell. Further analysis will be needed to determine whether RPA subcomplexes have distinct function(s) in the cell.

Previous studies have reported that RPA1 depletion results in the activation of checkpoint kinases ATM and Chk2 (14, 40). Dodson *et al.* (14) also reported that RPA1 depletion in HeLa cells leads to a G_2/M arrest and increased cell death, but they did not observe an accumulation of cells in S phase. In contrast, we observe that RPA1 depletion causes the majority of cells to accumulate in S phase, in addition to G_2/M arrest and subsequent cell death. There are several possible reasons for the differences observed between our studies and those of Dodson *et al.* (14). It is possible that there are differences in RPA1 depletion because of the different siRNA targets used; the coding region was targeted in Dodson *et al.* (14), whereas our siRNA targets the 3′-UTR. Alternatively, but not mutually exclusive, the phenotypic differences might be due to different knockdown efficiency or differences in cell culture conditions. We have found that cell culture conditions can have an effect on the severity of the phenotype observed. Seeding tissue culture wells with twice the number of cells results in a less pronounced S phase accumulation phenotype (data not shown). Presumably this observation is because the cells begin to reach confluence during the time course of the experiment, resulting in fewer cells actively proceeding through S phase. Therefore, it is possible that the growth conditions used by Dodson *et al.* (14) allowed cells to reach G_2/M more efficiently, thereby emphasizing that phenotype.

We believe that our studies reflect a true phenotype for depletion of RPA1 in cells for two reasons. First, we show that the siRNA used depletes RPA1 protein very efficiently. Second, we show that a GFP-tagged RPA1 can rescue the RPA1 knockdown phenotype, such that the cell cycle phenotype is indistinguishable from that of untransfected or mock-transfected cells. This confirms that our 3′-UTR targeting siRNA is targeting RPA1, and the mutant phenotype is due specifically to RPA1 depletion. Furthermore, our results are consistent with the prediction that RPA1 is essential for DNA replication and thus for progression through S phase.

The Contribution of ssDNA Binding to Cellular RPA Function—Residues in the core ssDNA-binding domain of RPA1, DBD-A and DBD-B, make multiple types of contacts with ssDNA. To understand the contributions of these interactions to ssDNA binding and cellular functions, we generated a series of mutant forms of RPA with varying numbers of mutations in polar residues that interact with DNA. Previously, it was observed that mutation of individual interacting residues in either DBD-A or DBD-B causes a significant decrease in ssDNA binding affinity. Combining two mutations generally causes a further reduction of binding (17). We show here that mutating polar residues Arg-234 and Arg-216 in addition to the two mutations in RPA1-DM (K263A and E277A) did not further reduce ssDNA binding affinity. Further mutation of R210A and W212A, to eliminate all polar residues that interact with DNA in DBD-A, leads to an additional order of magnitude decrease in ssDNA binding, suggesting three possibilities. First, mutation of interacting polar residues disrupts RPA-ssDNA interactions, reducing ssDNA binding affinity, but once some interactions have been disrupted, additional mutations have only a minimal effect. Second, the contributions of individual residues to ssDNA binding may be different. Third, the mutation of a substantial number of surface residues in a single domain may have a cumulative effect on the folding/structure of the DBD-A domain of RPA1, affecting ssDNA binding activity. Additional studies will be needed to distinguish between these possibilities.

When the DNA-binding domain mutants were examined in cells, it was found that all of the mutants, except for RPA1-CM, could rescue at least some of the replication defects observed when endogenous RPA1 is depleted. This was somewhat surprising, because the RPA1-DM, RPA1-TM, and RPA1-QM all decrease ssDNA binding by 100-fold compared with WT RPA1. In contrast, RPA1-CM showed no rescue of the RPA1-depletion phenotype when either the cell cycle distribution or localization to DNA damage was examined. Although RPA1-CM appears to be slightly less stable *in vitro*, our cellular data suggest that RPA1-CM is expressed similarly or better than RPA1-TM and RPA1-QM (both of which function similarly to WT RPA1). Therefore, we conclude that the inability to complement the RPA1 depletion defect is probably because of activity loss rather than reduced protein expression or stability. The simplest interpretation of these data is that RPA can function in the cell when ssDNA binding is substantially reduced (RPA1-DM); however, there is a "threshold" of binding (less than that of RPA1-DM) necessary for RPA function.

Mutation of Key Aromatic Residues of RPA1 Reveals the Importance of These Residues in DNA Repair and Cell Cycle Progression—RPA-ssDNA contacts also involve nonpolar base-stacking interactions mediated through specific aromatic residues. In yeast, mutation of the aromatic residues in DBD-A and DBD-B leads to the substantial ssDNA binding defects (63); however, for human RPA1, the contribution of these aromatic residues to ssDNA binding appears to be minimal compared with polar-interacting residues; mutation of any two of the conserved aromatic residues reduces binding by an order of magnitude or less (17, 19). With these modest effects on DNA binding, we predicted that these mutants would have a minimal effect on cellular function; however, this was not the case. Both RPA1-aroA and RPA1-aroB appear to support DNA replication to varying degrees but result in a significant arrest of cells in G_2/M phase. This indicates that RPA1-aroA and RPA1-aroB are able to rescue sufficient replication for the cells to get into G_2/M, but the cells are not able to proceed through G_2/M.

Why do these cells arrest in G_2/M? RPA is necessary for DNA repair; however, RPA1-aroA and RPA1-aroB are not detected at sites of DNA damage. This suggests that these mutants are defective in localization or in some process necessary for DNA repair and that this defect may be leading to the G_2/M arrest. Alternatively (or in addition), it is possible that replication is somewhat defective in these cells. If this is the case, then it is likely that incomplete replication triggers a cellular DNA-damage response that activates cellular checkpoints. Consistent with this is the observation that RPA1-aroA and RPA1-aroB lead to low but detectable γ-H2AX staining in otherwise unstressed cells. In *S. cerevisiae*, it has been reported that mutating key aromatic residues in DBD-A (Phe-238) or in DBD-B (Trp-360 and Phe-367) leads to inviability (28). It is possible that the inability to observe a colony (cell growth) for *rfa1-F238A* ("*rfa1-aroA*") or "*rfa1-W360A-F367A*" ("*rfa1-aroB*") yeast cells (perceived inviability) is because of checkpoint activation inhibiting cell division early in colony formation. If this mechanism is correct, we would predict that *rfa1-aroA* or *rfa1-aroB* might be viable in a checkpoint defective strain. We are currently examining this possibility.

The ssDNA binding activity of DBD-A and DBD-B aromatic mutants is more that 10-fold higher than RPA1-DM, which appears to be fully functional *in vivo*. Thus, the defects in RPA1-aroA and RPA1-aroB must either be caused by the loss of a specific function independent from ssDNA binding (*e.g.* a protein interaction) or the loss of an interaction between these residues and ssDNA, which is important for certain RPA functions and not for overall ssDNA binding affinity. Whatever the mechanism, these studies show that ssDNA binding affinity is not solely responsible for cell cycle phenotypes observed for mutations in DBD-A or DBD-B, and that RPA has an essential function that is independent of ssDNA binding affinity.

The prevalent G_2/M arrest suggests that the aromatic residue mutants have a defect somewhere between S phase and

cell division. It is interesting to note that RPA2 also becomes phosphorylated in this part of the cell cycle: during S phase and at G_2/M (65), because it has been reported that hyperphosphorylated RPA2 causes conformational changes in the RPA complex (53), including changes near the aromatic residue Trp-361 in DBD-B (66). It has also been demonstrated that RPA2 phosphorylation is necessary for formation of mitotic chromatin in *Xenopus* oocyte extracts (67). It is possible that the phosphorylated N-terminal domain of RPA2 causes changes near the aromatic residues in DBD-B (and possibly DBD-A), to allow for progression through G_2/M, and that mutation of these aromatic residues prohibits this change. Alternatively, there may be key protein interactions that are dependent on these aromatic residues, and disruption of these interactions results in activation of the G_2/M checkpoint.

DNA Binding Domain F of RPA1 Is Not Necessary for Replication but Is Necessary for the Response to DNA Damage—HeLa cells arrest in G_2/M in response to DNA damage-induced CPT or ETP treatment. When these cells are depleted for RPA1, a substantial portion of the cells accumulates in S phase similar to that observed in unstressed RPA1-depleted cells. This is presumably because cells cannot complete S phase in the absence of RPA1. In response to CPT or ETP, all of the DBD-A and DBD-B mutants mimic their respective cell cycle phenotypes after treatment (*i.e.* cells that have replication defects in unstressed cells also have replication defects in chemically stressed cells).

In contrast, DBD-F mutants perform replication indistinguishable from WT RPA in unstressed cells; however, after CPT or ETP treatment, there is a substantial proportion of cells in both G_1 and S phase. There are a number of plausible explanations for this observation. One explanation is that there is a defect in the G_2/M checkpoint activation in these cells, allowing progression through G_2/M back into G_1 and S phase. We do not favor this explanation, because at lower doses of CPT or ETP there is little or no detectable cell cycle phenotype in WT cells; however, an increase in G_2/M cells is always observed in RPA1-t11 and RPA1-ΔFL cells. A second possible explanation is that upon high levels of DNA damage (medium dose of CPT or ETP), there is a defect in progression into and through S phase for RPA1-t11 and RPA1-ΔFL cells. We do not favor this explanation either, because RPA1-t11, RPA1-ΔFL, and the other mutants (namely RPA1-aroA and RPA1-aroB) do not appear to have an added replication defect when DNA damage is present. However, this possibility cannot be completely ruled out. The explanation we favor involves adaptation. Adaptation is defined as initial checkpoint activation followed by eventual progression through the checkpoint after prolonged exposure to cellular stress, and it is thought to be a fail-safe pathway that allows cells a chance of survival in the presence of continuous DNA damage (68). RPA1-t11 and RPA1-ΔFL mutants cause G_2/M checkpoint activation upon exposure to a low dose of damage. Activation of the G_2/M checkpoint was also observed at higher doses of damage. The simplest explanation of the increased amounts of G_1 and S phase cells observed under these conditions is that prolonged exposure to this higher dose of DNA damage results in some cells "adapting" and escaping from the G_2/M checkpoint. These observations are consistent with the previous finding that *rfa1-t11* yeast strains display more adaptation than *RFA1* (WT) strains, and that *rfa1-t11* does suppress a number of adaptation-defective strains (30, 35). Adaptation is well characterized in yeast (68), and it has also been demonstrated to occur in human cells (69).

There is little contribution of DBD-F to ssDNA binding (32, 46), so this domain must be important for other processes involving RPA. Although Philipova *et al.* (28) demonstrated that deletion of more than the first 10 amino acids of this domain in yeast results in cell inviability, we have shown that RPA1-ΔFL in unstressed human cells appears to be indistinguishable from WT RPA1 and from RPA1-t11. Because RPA1-ΔFL and RPA1-t11 behave similarly, and *rfa1-t11* is viable in yeast, it is possible that yeast cells might be viable if the entire domain (DBD-F) is removed. We suggest that a protein containing part of the DBD-F (such as that in yeast) may result in inhibitory effects and therefore would be less functional. Supporting this conclusion is the finding that DBD-F is dispensable for DNA replication in the *in vitro* SV40 replication system (46). Interestingly, it has been demonstrated that a number of mutations in yeast leading to severe UV and methyl methanesulfonate sensitivity lie in DBD-F (20, 21). Furthermore, the *rfa1-t11* mutation (in DBD-F) in yeast leads to a defect in the G_2/M checkpoint (13), suggesting that the primary contribution of this domain is in response to DNA damage. In support of this, our data demonstrate that in otherwise unstressed cells, expression of RPA1-ΔFL rescues RPA1-depletion and does not lead to any detectable phenotypes or to detectable levels of γ-H2AX staining. This implies that this domain may only be necessary when cells are stressed.

Similar to yeast *rfa1-t11*, we have shown that RPA1-t11 and RPA-ΔF have the ability to localize to sites of DNA damage. This would indicate that DBD-F is not necessary for this step, and that any defect in DNA repair lies downstream of damage recognition. It has been demonstrated that a peptide mimicking phosphorylation of the N terminus of RPA2 can interact with DBD-F (53). Additionally, RPA interacts with a number of proteins (*e.g.* Rad51, Rad52, and XPA) necessary for DNA repair. The regions of RPA that interact with these proteins are predominantly the C terminus of RPA2 and the N terminus of RPA1 (3). Upon DNA damage, RPA2 is hyperphosphorylated (15), and there is an increase in the interactions between Rad51, Rad52, and XPA with RPA2 (70). These proteins also interact with the N-terminal region of RPA1 (3). In yeast, there is a defect in displacement of Rfa1-t11 from ssDNA by Rad51 (32) and a defect in meiotic double strand break processing (31). It is possible that mutations in DBD-F lead to disruption of an interaction(s) with repair/recombination proteins or an altered conformation of the RPA complex (perhaps caused by a disruption between the RPA2 N terminus and the RPA1 N terminus) that leads to the observed repair and cell cycle defects. Finally, depletion of RPA1 leads to an inability to load the 9-1-1 complex onto damaged DNA (42). Furthermore, in yeast, *rfa1-t11* inhibits recruitment of Rad17 to DNA damage (64), and it has been proposed that this

would result in a defect in cell cycle regulation. We propose that the lack of functional DBD-F is solely responsible for these phenotypes, and this explains why RPA1-t11 and RPA1-ΔFL have similar phenotypes.

We have shown here that the knockdown and replacement strategy is a powerful tool for correlating *in vitro* properties and identifying the contributions of each domain of RPA with cellular function in human cells. These studies demonstrate that mutations in RPA lead to defects in RPA functions that can be independent of their ssDNA binding activity, and that specific domains (*e.g.* DBD-F) or specific types of mutations (*e.g.* RPA1-aroA and RPA1-aroB) show defects in only some cellular functions of RPA. These results show that ssDNA binding activity is essential for DNA replication, and that ssDNA binding and an additional activity (or activities) are needed for DNA repair and cell cycle progression. This system will allow for the further characterization of human RPA and for the identification of the contributions of each subunit, domain, and region to RPA function in the context of the cell.

Acknowledgments—We thank John Harty and Jodie Haring for instruction and access to the FACSCalibur and Timothy Moss, Yan Jiang, and David Price for tissue culture assistance and access to the fluorescence microscope. We thank the Wold laboratory for scientific discussions and critical reading of this manuscript.

REFERENCES

1. Wold, M. S. (1997) *Annu. Rev. Biochem.* **66,** 61–92
2. Iftode, C., Daniely, Y., and Borowiec, J. A. (1999) *CRC Crit. Rev. Biochem.* **34,** 141–180
3. Fanning, E., Klimovich, V., and Nager, A. R. (2006) *Nucleic Acids Res.* **34,** 4126–4137
4. Ishibashi, T., Kimura, S., and Sakaguchi, K. (2006) *J Biochem.* (*Tokyo*) **139,** 99–104
5. Kumaran, S., Kozlov, A. G., and Lohman, T. M. (2006) *Biochemistry* **45,** 11958–11973
6. Kim, C., Snyder, R. O., and Wold, M. S. (1992) *Mol. Cell. Biol.* **12,** 3050–3059
7. Salas, T. R., Petruseva, I., Lavrik, O., Bourdoncle, A., Mergny, J. L., Favre, A., and Saintome, C. (2006) *Nucleic Acids Res.* **34,** 4857–4865
8. Gao, H., Cervantes, R. B., Mandell, E. K., Otero, J. H., and Lundblad, V. (2007) *Nat. Struct. Mol. Biol.* **14,** 208–214
9. Wobbe, C. R., Weissbach, L., Borowiec, J. A., Dean, F. B., Murakami, Y., Bullock, P., and Hurwitz, J. (1987) *Proc. Natl. Acad. Sci. U. S. A.* **84,** 1834–1838
10. Fairman, M. P., and Stillman, B. (1988) *EMBO J.* **7,** 1211–1218
11. Wold, M. S., and Kelly, T. (1988) *Proc. Natl. Acad. Sci. U. S. A.* **85,** 2523–2527
12. Schramke, V., Luciano, P., Brevet, V., Guillot, S., Corda, Y., Longhese, M. P., Gilson, E., and Geli, V. (2004) *Nat. Genet.* **36,** 46–54
13. Kim, H. S., and Brill, S. J. (2001) *Mol. Cell. Biol.* **21,** 3725–3737
14. Dodson, G. E., Shi, Y., and Tibbetts, R. S. (2004) *J. Biol. Chem.* **279,** 34010–34014
15. Binz, S. K., Sheehan, A. M., and Wold, M. S. (2004) *DNA Repair* (*Amst.*) **3,** 1015–1024
16. Bochkarev, A., and Bochkareva, E. (2004) *Curr. Opin. Struct. Biol.* **14,** 36–42
17. Wyka, I. M., Dhar, K., Binz, S. K., and Wold, M. S. (2003) *Biochemistry* **42,** 12909–12918
18. Arunkumar, A. I., Stauffer, M. E., Bochkareva, E., Bochkarev, A., and Chazin, W. J. (2003) *J. Biol. Chem.* **278,** 41077–41082
19. Walther, A. P., Gomes, X. V., Lao, Y., Lee, C. G., and Wold, M. S. (1999) *Biochemistry* **38,** 3963–3973
20. Umezu, K., Sugawara, N., Chen, C., Haber, J. E., and Kolodner, R. D. (1998) *Genetics* **148,** 989–1005
21. Longhese, M. P., Neecke, H., Paciotti, V., Lucchini, G., and Plevani, P. (1996) *Nucleic Acids Res.* **24,** 3533–3537
22. Braun, K. A., Lao, Y., He, Z., Ingles, C. J., and Wold, M. S. (1997) *Biochem.* **36,** 8443–8454
23. Gomes, X. V., and Wold, M. S. (1995) *J. Biol. Chem.* **270,** 4534–4543
24. Lao, Y., Gomes, X. V., Ren, Y. J., Taylor, J. S., and Wold, M. S. (2000) *Biochemistry* **39,** 850–859
25. Pestryakov, P. E., Khlimankov, D. Y., Bochkareva, E., Bochkarev, A., and Lavrik, O. I. (2004) *Nucleic Acids Res.* **32,** 1894–1903
26. Bochkareva, E., Frappier, L., Edwards, A. M., and Bochkarev, A. (1998) *J. Biol. Chem.* **273,** 3932–3936
27. Bochkarev, A., Bochkareva, E., Frappier, L., and Edwards, A. M. (1999) *EMBO J.* **18,** 4498–4504
28. Philipova, D., Mullen, J. R., Maniar, H. S., Gu, C., and Brill, S. J. (1996) *Genes Dev.* **10,** 2222–2233
29. Parker, A., Gu, Y. S., Mahoney, W., Lee, S. H., Singh, K. K., and Lu, A. L. (2001) *J. Biol. Chem.* **276,** 5547–5555
30. Tuteja, N., and Tuteja, R. (2001) *CRC Crit. Rev. Biochem. Mol. Biol.* **36,** 261–290
31. Soustelle, C., Vedel, M., Kolodner, R., and Nicolas, A. (2002) *Genetics* **161,** 535–547
32. Kantake, N., Sugiyama, T., Kolodner, R. D., and Kowalczykowski, S. C. (2003) *J. Biol. Chem.* **278,** 23410–23417
33. Zou, L., and Elledge, S. J. (2003) *Science* **300,** 1542–1548
34. Wang, X., and Haber, J. E. (2004) *PLoS Biol.* **2,** E21
35. Lee, S. E., Pellicioli, A., Vaze, M. B., Sugawara, N., Malkova, A., Foiani, M., and Haber, J. E. (2003) *Mol. Cell. Biol.* **23,** 8913–8923
36. Sugiyama, T., Kantake, N., Wu, Y., and Kowalczykowski, S. C. (2006) *EMBO J.* **25,** 5539–5548
37. Majka, J., Binz, S. K., Wold, M. S., and Burgers, P. M. (2006) *J. Biol. Chem.* **281,** 27855–27861
38. Kanoh, Y., Tamai, K., and Shirahige, K. (2006) *Gene* (*Amst.*) **377,** 88–95
39. Grandin, N., and Charbonneau, M. (2007) *Nucleic Acids Res.* **35,** 821–838
40. Araya, R., Hirai, I., Meyerkord, C. L., and Wang, H. G. (2005) *FEBS Lett.* **579,** 157–161
41. Niida, H., and Nakanishi, M. (2006) *Mutagenesis* **21,** 3–9
42. Wu, X., Shell, S. M., and Zou, Y. (2005) *Oncogene* **24,** 4728–4735
43. Kenny, M. K., Schlegel, U., Furneaux, H., and Hurwitz, J. (1990) *J. Biol. Chem.* **265,** 7693–7700
44. Erdile, L. F., Wold, M. S., and Kelly, T. J. (1990) *J. Biol. Chem.* **265,** 3177–3182
45. Henricksen, L. A., Umbricht, C. B., and Wold, M. S. (1994) *J. Biol. Chem.* **269,** 11121–11132
46. Gomes, X. V., and Wold, M. S. (1996) *Biochemistry* **35,** 10558–10568
47. Binz, S. K., Dickson, A. M., Haring, S. J., and Wold, M. S. (2006) *Methods Enzymol.* **409,** 11–38
48. Kim, C., Paulus, B. F., and Wold, M. S. (1994) *Biochemistry* **33,** 14197–14206
49. Liu, P. K., Chang, C. C., Trosko, J. E., Dube, D. K., Martin, G. M., and Loeb, L. A. (1983) *Proc. Natl. Acad. Sci. U. S. A.* **80,** 797–801
50. Sarkaria, J. N., Busby, E. C., Tibbetts, R. S., Roos, P., Taya, Y., Karnitz, L. M., and Abraham, R. T. (1999) *Cancer Res.* **59,** 4375–4382
51. Pfuetzner, R. A., Bochkarev, A., Frappier, L., and Edwards, A. M. (1997) *J. Biol. Chem.* **272,** 430–434
52. Bochkarev, A., Pfuetzner, R. A., Edwards, A. M., and Frappier, L. (1997) *Nature* **385,** 176–181
53. Binz, S. K., Lao, Y., Lowry, D. F., and Wold, M. S. (2003) *J. Biol. Chem.* **278,** 35584–35591
54. Golub, E. I., Gupta, R. C., Haaf, T., Wold, M. S., and Radding, C. M. (1998) *Nucleic Acids Res.* **26,** 5388–5393
55. Vassin, V. M., Wold, M. S., and Borowiec, J. A. (2004) *Mol. Cell. Biol.* **24,** 1930–1943
56. Avemann, K., Knippers, R., Koller, T., and Sogo, J. M. (1988) *Mol. Cell. Biol.* **8,** 3026–3034
57. Liu, L. F., Duann, P., Lin, C. T., D'Arpa, P., and Wu, J. X. (1996) *Ann. N. Y. Acad. Sci.* **803,** 44–49

58. Hande, K. R. (1998) *Eur. J. Cancer* **34,** 1514–1521
59. Paull, T. T., Rogakou, E. P., Yamazaki, V., Kirchgessner, C. U., Gellert, M., and Bonner, W. M. (2000) *Curr. Biol.* **10,** 886–895
60. Deng, X., Habel, J. E., Kabaleeswaran, V., Snell, E. H., Wold, M. S., and Borgstahl, G. E. (2007) *J. Mol. Biol.* **374,** 865–876
61. Murti, K. G., He, D. C., Brinkley, B. R., Scott, R., and Lee, S. H. (1996) *Exp. Cell Res.* **223,** 279–289
62. Dimitrova, D. S., and Gilbert, D. M. (2000) *Exp. Cell Res.* **254,** 321–327
63. Bastin-Shanower, S. A., and Brill, S. J. (2001) *J. Biol. Chem.* **276,** 36446–36453
64. Zou, L., Liu, D., and Elledge, S. J. (2003) *Proc. Natl. Acad. Sci. U. S. A.* **100,** 13827–13832
65. Fotedar, R., and Roberts, J. M. (1992) *EMBO* **11,** 2177–2187
66. Liu, Y., Kvaratskhelia, M., Hess, S., Qu, Y., and Zou, Y. (2005) *J. Biol. Chem.* **280,** 32775–32783
67. Cuvier, O., Lutzmann, M., and Mechali, M. (2006) *Curr. Biol.* **16,** 516–523
68. Galgoczy, D. J., and Toczyski, D. P. (2001) *Mol. Cell. Biol.* **21,** 1710–1718
69. Syljuasen, R. G. (2007) *Oncogene* **26,** 5833–5839
70. Wu, X., Yang, Z., Liu, Y., and Zou, Y. (2005) *Biochem. J.* **391,** 473–480